

DYNAMIC MODELLING OF MULTIVARIATE DIMENSIONS AND THEIR TEMPORAL RELATIONSHIPS USING LATENT PROCESSES: APPLICATION TO ALZHEIMER'S DISEASE

Bachirou O. Taddé^{1,*}, Hélène Jacqmin-Gadda¹, Jean-François Dartigues¹, Daniel Commenges¹,
Cécile Proust-Lima¹ for the Alzheimer's Disease Neuroimaging Initiative[†]

¹ INSERM, UMR1219, Univ. Bordeaux, F33000 Bordeaux, France

* oladedji-bachirou.tadde@u-bordeaux.fr

[†]*Data used in preparation of this article were obtained from the Alzheimer's Disease Neuroimaging Initiative (ADNI) database (adni.loni.usc.edu). As such, the investigators within the ADNI contributed to the design and implementation of ADNI and/or provided data but did not participate in analysis or writing of this report. A complete listing of ADNI investigators can be found at: http://adni.loni.usc.edu/wp-content/uploads/show_to_apply/ADNI_Acknowledgement_List.pdf*

Abstract

Alzheimer's disease gradually affects several components including the cerebral dimension with brain atrophies, the cognitive dimension with a decline in various functions and the functional dimension with impairment in the daily living activities. Understanding how such dimensions interconnect is crucial for AD research. However it requires to simultaneously capture the dynamic and multidimensional aspects, and to explore temporal relationships between dimensions. We propose an original dynamic structural model that accounts for all these features. The model defines dimensions as latent processes and combines a multivariate linear mixed model and a system of difference equations to model trajectories and temporal relationships between latent processes in finely discrete time. Dimensions are simultaneously related to their observed (possibly multivariate) markers through nonlinear equations of observation. Parameters are estimated in the maximum likelihood framework enjoying a closed form for the likelihood. We demonstrate in a simulation study that this dynamic model in discrete time benefits the same causal interpretation of temporal relationships as models defined in continuous time as long as the discretization step remains small. The model is then applied to the data of the Alzheimer's Disease Neuroimaging Initiative. Three longitudinal dimensions (cerebral anatomy, cognitive ability and functional autonomy) measured by 6 markers are analyzed and their temporal structure is contrasted between different clinical stages of Alzheimer's disease.

Keywords. causality, difference equations, latent process, longitudinal data, mixed models, multivariate data.

1 Introduction

Dementia is a general syndrome characterized by a long term and gradual decrease in the ability to think and remember with consequences on the person’s daily functioning. It represents a pressing public health problem with an estimated worldwide prevalence of 46.8 millions cases and health care burden with US \$ 817.9 billions in 2015 (Wimo et al., 2017). Alzheimer disease (AD), the most common form of dementia (60% to 80% of the cases, Reitz and Mayeux (2014)), gradually affects multiple components long before clinical diagnosis with brain atrophies, cognitive decline in various functions (memory, language, orientation in space and time, etc.) and loss of autonomy in daily living activities.

Although essential for the assessment of compounds and more generally for AD research, knowledge of the natural history of AD and its progression is still imprecise. Theoretical schemes have highlighted its expected dynamic and multidimensional aspects. For instance, Jack et al. (2013) hypothesized a sequence with the accumulation of proteins in the brain (amyloid- β and τ proteins), the atrophy of brain regions (e.g., hippocampus) and then clinical manifestations with cognitive and functional declines on which dementia diagnosis currently relies. However, this theory is hard to translate into a statistical model because it requires combining multidimensional and dynamic aspects, and exploring temporal relationships between dimensions.

As in other medical contexts, the dynamic aspect of AD has been mostly apprehended using mixed models in which one dimension is analyzed according to time and covariates (Amieva et al., 2008; Donohue et al., 2014). This approach naturally handles dynamic processes by modeling in continuous time the process underlying the repeated discrete observations. To emphasize the distinction between the true process of interest from its noisy observations, mixed models can be split into a structural model which analyzes the latent process over time, and equations of observations which simultaneously link the unobserved quantity to the noisy observed outcomes at each visit (Proust-Lima et al., 2013). With such split, mixed models can treat one or more markers indiscriminately, as long as they measure the same latent quantity. This is particularly useful for dimensions such as cognition measured by a battery of neuropsychological tests or cerebral anatomy measured by regional volumes.

To understand how dimensions are inter-related in AD, some have explored pre-determined relationships by examining change over time of one biomarker according to another one and assumed the latter was observed without measurement error (e.g., Landau et al. (2011); Han et al. (2012)). This approach quantifies temporal relationships but it relies on a specific *a priori* determined sequence and does not consider all biomarkers as continuous processes. Others used bivariate mixed models to dynamically model two dimensions and account for their correlation through correlated random effects (e.g., Mungas et al. (2005); Robitaille et al. (2012)). However such models remain descriptive; they account for the correlation between the markers but do not allow to distinguish the influence of each marker on the other.

Temporal asymmetric relationships between processes have been mainly apprehended with Dynamic Bayesian Networks (DBN), Dynamic Structural Equations Modelling (DSEM) and Cross-Lagged Models (CLM) (Song et al., 2009; Hamaker et al., 2015). These approaches extend the concept of Directed Acyclic Graphs (DAG) (Greenland, 2000) to longitudinal data by modelling temporal relationships between successive states of a network of processes. Although they account for the longitudinal data structure and the measurement sequence, these methods have two main drawbacks that this contribution intends to circumvent. First, the definition of the model most often depends on the discrete visit process, so that time associations are limited to those between successive observed visits (Hamaker et al., 2015; Kuiper and Ryan, 2018; Voelkle et al., 2018). This can lead to biased results in case of unequal time intervals. Even when observations are equally-spaced (generally in grossly discrete time), or when the time elapsed between visits is taken into account through time-dependent parameters, the estimated lagged effects are still specific to the discrete time intervals used in the study and spurious causal temporal associations might appear as recently demonstrated (Aalen et al., 2016). The second and main drawback of these methods is that they quantify the association between successive levels of the processes while we are mainly interested by the influence of each process on the subsequent change of other processes. Yet a dynamic view of causality would seek local dependence structures linking the network of processes to its infinitesimal subsequent change over time (Aalen and Frigessi, 2007; Didelez, 2008; Commenges and Gégout-Petit, 2009) in order to retrieve the mechanism which explains how the system changes as time changes (Voelkle et al., 2018). Local dependence structures can be naturally investigated with mechanistic models which relate a system of processes over time using differential equations. Proposed notably in HIV studies (Prague et al., 2017), they allow retrieving causal associations between disease components. Yet mechanistic models are numerically very demanding so that their application to complex diseases such as AD is compromised. In addition they require precise biological knowledge which lacks for AD.

Our objective is thus to propose a statistical model that simultaneously describes the dynamics of multiple dimensions involved in AD and assesses their temporal relationships similarly as in a mechanistic model but with much less numerical complexity. We consider a system of latent dimensions possibly observed through one or several longitudinal markers. We define a set of difference equations to model the change over a discretized time of the system according to its previous state. Yet in contrast with other methods (DBN, DSEM, CLM), this discretization step is disconnected from the observation process and can be finely chosen. As discretization might still distort the causal interpretations of temporal relationships compared to a model in continuous time, we specifically evaluate the impact of discretization on the temporal influence structure in a simulation study. The methodology is applied to the Alzheimer’s Disease Neuroimaging Initiative database to explore the temporal structure between cerebral, cognitive and functional dimensions at different stages of AD.

2 Motivating Data

Data were obtained from the Alzheimer’s Disease Neuroimaging Initiative (ADNI) database (adni.loni.usc.edu). The ADNI was launched in 2003 with the primary goal to test whether serial magnetic resonance imaging (MRI), positron emission tomography (PET), other biological markers, and clinical and neuropsychological assessment could be combined to measure the progression of mild cognitive impairment (MCI) and early Alzheimer’s disease (AD). We focused on the ADNI 1 phase (Mueller et al., 2005), a multisite observational study that included $N \approx 800$ individuals aged 55-90 enrolled in three stages of progression to AD: normal aging (CN, $N \approx 200$), mild cognitive impairment (MCI, $N \approx 400$), and diagnosed Alzheimer’s Disease (dAD, $N \approx 200$). Participants were followed-up every 6 months up to 3 years for CN and MCI groups and up to 2 years for the dAD group (except at month 18 for dAD and CN, and at month 30 for CN and MCI). At each visit, information was collected, including for the present work, volumes of brain regions measured by MRI, a battery of 19 cognitive scores and a functional assessment.

3 Methodology

3.1 Structural model for the system of latent processes

Consider D latent processes $\mathbf{\Lambda}_i(t)_{t \geq 0}$ (with $\mathbf{\Lambda}_i(t) = (\Lambda_i^d(t))_{d=1, \dots, D}^\top$) representing a system of D dimensions (e.g. $D = 3$ for cerebral anatomy, cognitive ability and functional autonomy dimensions in AD) for individual i with $i = 1, \dots, N$. We assume $\mathbf{\Lambda}_i(t)_{t \geq 0}$ is defined at discrete times $t_j = j \times \delta$ with $j \in \tau = \{0, 1, \dots, J\}$, and δ a constant discretization step. Let us denote $\Delta \mathbf{\Lambda}_i(t_j + \delta) = \mathbf{\Lambda}_i(t_j + \delta) - \mathbf{\Lambda}_i(t_j)$ the change of the system between two successive times and $\frac{\Delta \mathbf{\Lambda}_i(t_j + \delta)}{\delta}$ the rate of change of the system.

To make explicit the modelling of the temporal relationships, we split the structural model into two multivariate linear mixed submodels for: (i) the level of the processes at baseline $\mathbf{\Lambda}_i(0)$ and (ii) the rate of change of the system over time $\frac{\Delta \mathbf{\Lambda}_i(t_j + \delta)}{\delta}$ using difference equations:

$$\begin{cases} \mathbf{\Lambda}_i(0) = \mathbf{X}_i^0 \boldsymbol{\beta} + \mathbf{u}_i \\ \frac{\Delta \mathbf{\Lambda}_i(t_j + \delta)}{\delta} = \mathbf{X}_i(t_j + \delta) \boldsymbol{\gamma} + \mathbf{Z}_i(t_j + \delta) \mathbf{v}_i + \mathbf{A}_{i, \delta}(t_j) \mathbf{\Lambda}_i(t_j) \end{cases} \quad (1)$$

where \mathbf{X}_i^0 is the $D \times p_0$ -matrix of covariates associated with the p_0 -vector of fixed effects $\boldsymbol{\beta}$, and \mathbf{u}_i is the D -vector of individual random intercepts u_i^d in the initial system $\mathbf{\Lambda}_i(0)$. The $(D \times p)$ -matrix \mathbf{X}_i and the $(D \times q)$ -matrix \mathbf{Z}_i include time-dependent covariates associated with the p -vector of fixed effects $\boldsymbol{\gamma}$ and the q -vector ($q = \sum_{d=1}^D q_d$) of individual random effects $\mathbf{v}_i = (v_i^d)_{d=1, \dots, D}$, respectively. $\mathbf{A}_{i, \delta}$ is the $D \times D$ -matrix of temporal influences.

For each process Λ_i^d , the $(q_d + 1)$ vector of individual random effects $(u_i^d, v_i^d)^\top$ is assumed to have a multivariate normal distribution with variance-covariance matrix $\begin{pmatrix} b_u^{d^2} & \mathbf{B}_{uv}^d \\ \mathbf{B}_{uv}^{d \top} & \mathbf{B}_v^d \end{pmatrix}$ where \mathbf{B}_{uv}^d and

\mathbf{B}_v^d are unstructured. We assume that random effects may be correlated within each process d (to take into account inter-individual variability in each process trajectory) and between processes at baseline (to take into account the possible within-individual correlation between processes due to anterior dependencies). Other correlations between random effects are kept null to ensure that the temporal relationships are entirely captured by matrix $\mathbf{A}_{i,\delta}$. Consequently the entire $(D + q)$ -vector of individual random effects $\mathbf{w}_i = (\mathbf{u}_i^\top, \mathbf{v}_i^\top)^\top$ has a multivariate normal distribution,

$$\mathbf{w}_i \sim \mathcal{N} \left(\begin{pmatrix} \mathbf{0} \\ \mathbf{0} \end{pmatrix}, \mathbf{B} = \begin{pmatrix} \mathbf{B}_u & \mathbf{B}_{uv} \\ \mathbf{B}_{uv}^\top & \mathbf{B}_v \end{pmatrix} \right).$$

with \mathbf{B}_u the variance covariance matrix of \mathbf{u}_i , \mathbf{B}_v the D-block diagonal matrix with d^{th} block \mathbf{B}_v^d , and \mathbf{B}_{uv} the $D \times q$ matrix with d^{th} row $\left(\mathbf{O}_{\sum_{l=1}^{d-1} q_l}, \mathbf{B}_{uv}^d, \mathbf{O}_{\sum_{l=d+1}^D q_l} \right)$ where \mathbf{O}_x is the x -row vector of zeros. In the estimation process, \mathbf{B} is replaced by its Cholesky decomposition: $\mathbf{B} = \mathbf{L}\mathbf{L}^\top$, where \mathbf{L} is a $(D + q) \times (D + q)$ lower triangular matrix.

As in any latent variable model, the dimensions of the latent processes have to be defined to reach identifiability. Since we do not want to constrain the measurement models (in Section 3.2), we chose to standardize the latent processes at baseline by excluding intercepts from \mathbf{X}_i^0 (i.e., the processes have zero mean in the reference group at baseline) and fixing the variances of \mathbf{u}_i at one ($b_u^d = 1 \forall d \in \{1, \dots, D\}$).

The temporal influences between processes are modelled through the $D \times D$ -matrix of time-dependent effects $\mathbf{A}_{i,\delta}(t_j)$:

$$\mathbf{A}_{i,\delta}(t_j) = \begin{pmatrix} a_{i,11}(t_j) & \dots & a_{i,1d}(t_j) & \dots & a_{i,1D}(t_j) \\ \vdots & \ddots & \vdots & \ddots & \vdots \\ a_{i,d1}(t_j) & \dots & a_{i,dd}(t_j) & \dots & a_{i,dD}(t_j) \\ \vdots & \ddots & \vdots & \ddots & \vdots \\ a_{i,D1}(t_j) & \dots & a_{i,Dd}(t_j) & \dots & a_{i,DD}(t_j) \end{pmatrix}$$

This matrix captures the directed temporal influences between latent processes at time t_j and subsequent rates of change of latent processes between times t_j and $t_j + \delta$. Specifically, coefficient $a_{i,dd'}(t_j)$ quantifies the temporal effect of process d' at time t_j on process d . Each effect can be modelled according to time/covariates through a linear regression $a_{i,dd'}(t_j) = \mathbf{R}_i^\top(t_j) \boldsymbol{\alpha}_{dd'}$ where $\mathbf{R}_i(t_j)$ is a r-vector of time-dependent covariates associated with the r-vector of regression coefficients $\boldsymbol{\alpha}_{dd'}^\top = (\alpha_{dd'}^m)_{m=0, (r-1)}^\top$.

When the discretization step is not too large, the temporal influences intend to have the same causal interpretations as those of a model in continuous time (see Simulation Study 2).

3.2 Measurement Models of the longitudinal markers

Consider K ($K \geq D$) continuous longitudinal markers $\mathbf{Y}_{ij} = (Y_{ijk})_{k=1, \dots, K}^\top$ that have been measured for subject i at $(n_i + 1)$ continuous times $t_{ijk}^* \in [t_j, t_{j+1})$ with t_j the corresponding discretized time

and $j \in \tau_i$, with τ_i being any subset of τ of length $(n_i + 1)$. By considering $\tau_i \subset \tau$, we can consider observations sparser than the grid of discretized times.

Following Proust-Lima et al. (2013), we assume that the latent process $\mathbf{\Lambda}_i^d$ is the underlying common factor of K_d markers ($K = \sum_{d=1}^D K_d$) and we note \mathcal{K}^d the set of marker subscripts associated with latent process Λ_i^d . We assume that a marker measures only one latent process.

The link between a marker and its underlying latent process is defined by a marker-specific measurement model. If marker Y_{ijk} is Gaussian, the measurement model is a linear equation:

$$\frac{Y_{ijk} - \eta_{0k}}{\eta_{1k}} = \tilde{Y}_{ijk} = \Lambda_i^d(t_j) + \tilde{\epsilon}_{ijk}, \quad \forall k \in \mathcal{K}^d \text{ and } \forall j \in \tau_i, \quad (2)$$

where the vector of transformation parameters $\boldsymbol{\eta}_k = (\eta_{0k}, \eta_{1k})^\top$ is used to get the standardized form \tilde{Y}_{ijk} of the marker and $\tilde{\epsilon}_{ijk}$ are independent Gaussian errors with variance σ_k^2 .

In the more general case of a continuous marker (possibly non Gaussian), one may consider a nonlinear observation equation:

$$H_k(Y_{ijk}; \boldsymbol{\eta}_k) = \tilde{Y}_{ijk} = \Lambda_i^d(t_j) + \tilde{\epsilon}_{ijk}, \quad \forall k \in \mathcal{K}^d \text{ and } \forall j \in \tau_i, \quad (3)$$

where the link transformation H_k comes from a family of monotonic increasing and continuous functions parameterized with $\boldsymbol{\eta}_k$. Again \tilde{Y}_{ijk} is the transformed marker and $\tilde{\epsilon}_{ijk}$ are independent Gaussian errors with variance σ_k^2 . The link transformation H_k can be defined from a basis of I-splines (which are integrated M-splines (Ramsay, 1988)) in association with positive coefficients, thus providing an increasing bijective flexible transformation. We used here a quadratic I-splines basis with p_k internal knots, $(\mathbb{I}_m)_{m=1, p_k+3}$, so that

$$H_k(Y_{ijk}; \boldsymbol{\eta}_k) = \tilde{Y}_{ijk} = \eta_{0k} + \sum_{m=1}^{p_k+3} \eta_{mk}^2 \mathbb{I}_m(Y_{ijk}), \quad (4)$$

with $(\eta_{mk})_{m=0, p_k+3}$ the vector of parameters of the transformation. Since we constrained the latent processes dimensions, $\boldsymbol{\eta}_k$ does not need to be constrained to reach model identifiability.

In the following, we denote $\boldsymbol{\Sigma} = \text{diag}((\sigma_k^2)_{k=1, \dots, K})$ the diagonal variance matrix of the vector of errors $\tilde{\boldsymbol{\epsilon}}_{ij} = (\tilde{\epsilon}_{ijk})_{k=1, \dots, K}^\top$ and $\boldsymbol{\eta} = (\boldsymbol{\eta}_k^\top)_{\{1, \dots, K\}}^\top$, the total vector of transformation parameters for the K markers. The vector of transformed markers $\tilde{\mathbf{Y}}_{ij}$ is mapped to the system of latent processes $\mathbf{\Lambda}_i(t_j)$ through a $K \times D$ matrix \mathbf{P} with element (k, d) equal to 1 if marker k measures latent process d and zero otherwise:

$$\tilde{\mathbf{Y}}_{ij} = \mathbf{P} \mathbf{\Lambda}_i(t_j) + \boldsymbol{\epsilon}_{ij} \quad (5)$$

In practice the observation process may include intermittent missing observations for a subset of markers or for all the markers at any occasion $j \in \tau_i$, so that $K_{ij}^* \leq K$ markers are actually observed

at occasion j for subject i . Following the mixed model theory, we assume that observations are missing at random and note $\tilde{\mathbf{Y}}_{ij}^*$ the transformations of the actual K_{ij}^* -vector of observed markers \mathbf{Y}_{ij}^* at occasion j . The model linking the processes $\mathbf{\Lambda}_i(t_j)$ to the transformed markers $\tilde{\mathbf{Y}}_{ij}^*$ can be easily adapted to the presence of intermittent missing data by considering a $K_{ij}^* \times K$ observation matrix \mathbf{M}_{ij} where element (k^*, k) equals 1 if marker k is the k^{th} observed marker at occasion j and 0 if not for $k = 1, \dots, K$ and $k^* = 1, \dots, K_{ij}^*$:

$$\tilde{\mathbf{Y}}_{ij}^* = \mathbf{M}_{ij} \mathbf{P} \mathbf{\Lambda}_i(t_j) + \boldsymbol{\epsilon}_{ij}^* \quad (6)$$

with $\boldsymbol{\epsilon}_{ij}^*$ the vector of independent Gaussian errors with covariance matrix $\mathbf{M}_{ij} \boldsymbol{\Sigma} \mathbf{M}_{ij}^\top$.

3.3 Estimation by maximum likelihood

3.3.1 Distribution of the Latent Processes and transformed observations

Although the model was introduced through two submodels, the marginal distribution of latent processes (and by extension of the transformed observations) can be easily computed. By recurrence, the structural model (1) can be rewritten:

$$\left\{ \begin{array}{ll} \mathbf{\Lambda}_i(t_j) = \mathbf{X}_i^{(0)} \boldsymbol{\beta} + \mathbf{u}_i & \text{if } j = 0 \\ \mathbf{\Lambda}_i(t_j) = \tilde{\mathbf{A}}_{i,\delta}(0) \left\{ \mathbf{X}_i^{(0)} \boldsymbol{\beta} + \mathbf{u}_i \right\} + \delta \left\{ \mathbf{X}_i(t_{ij}) \boldsymbol{\gamma} + \mathbf{Z}_i(t_{ij}) \mathbf{v}_i \right\} & \text{if } j = 1 \\ \mathbf{\Lambda}_i(t_j) = \prod_{l=0}^{j-1} \tilde{\mathbf{A}}_{i,\delta}(t_l) \left\{ \mathbf{X}_i^{(0)} \boldsymbol{\beta} + \mathbf{u}_i \right\} + \delta \left\{ \mathbf{X}_i(t_j) \boldsymbol{\gamma} + \mathbf{Z}_i(t_j) \mathbf{v}_i \right\} & \text{if } j > 1 \\ \quad + \delta \sum_{s=1}^{j-1} \prod_{l=s}^{j-1} \tilde{\mathbf{A}}_{i,\delta}(t_l) \left\{ \mathbf{X}_i(t_s) \boldsymbol{\gamma} + \mathbf{Z}_i(t_s) \mathbf{v}_i \right\} & \end{array} \right. \quad (7)$$

where $t_j = j \times \delta$ for $j \in \tau$ and $\tilde{\mathbf{A}}_{i,\delta}(t_j) = \mathbf{I}_D + \delta \mathbf{A}_{i,\delta}(t_j)$.

By introducing $\boldsymbol{\Psi}_{i,\delta}(t_0, j, s)$ for $t_0 \geq 0$ and $s \leq j$ so that

$$\boldsymbol{\Psi}_{i,\delta}(t_0, j, s) = \begin{cases} \mathbf{I}_D, & \text{if } s = j \\ \prod_{l=s}^{j-1} \tilde{\mathbf{A}}_{i,\delta}(t_0 + t_l) & \text{if } s < j \end{cases} \quad (8)$$

Equation (7) can be rewritten

$$\mathbf{\Lambda}_i(t_j) = \boldsymbol{\Psi}_{i,\delta}(0, j, 0) \left(\mathbf{X}_i^{(0)} \boldsymbol{\beta} + \mathbf{u}_i \right) + \left[\delta \sum_{s=1}^j \boldsymbol{\Psi}_{i,\delta}(0, j, s) \left\{ \mathbf{X}_i(t_s) \boldsymbol{\gamma} + \mathbf{Z}_i(t_s) \mathbf{v}_i \right\} \right] \mathbf{1}_{\{j>0\}} \quad (9)$$

From this equation, it can be seen that the structural model is a specific nonlinear mixed model depending on individual random effects $\mathbf{w}_i = (\mathbf{u}_i^\top, \mathbf{v}_i^\top)^\top$. The vector $\mathbf{\Lambda}_i(t_j)$ has a multivariate normal

distribution with expectation $\boldsymbol{\mu}_{\Lambda_{ij}}$ and variance covariance matrix $\mathbf{V}_{\Lambda_{ijj}} = \text{var}\{\boldsymbol{\Lambda}_i(t_j)\}$, and the vector $\boldsymbol{\Lambda}_i = (\boldsymbol{\Lambda}_i(t_j)^\top)_{j \in \tau}^\top$ has a multivariate normal distribution with expectation $\boldsymbol{\mu}_{\boldsymbol{\Lambda}_i} = (\boldsymbol{\mu}_{\Lambda_{ij}}^\top)_{j \in \tau}^\top$ and variance-covariance matrix $\mathbf{V}_{\boldsymbol{\Lambda}_i} = (\mathbf{V}_{\Lambda_{ijj'}})_{(j,j') \in \tau^2}$ where

$$\boldsymbol{\mu}_{\Lambda_{ij}} = E\{\boldsymbol{\Lambda}_i(t_j)\} = \boldsymbol{\Psi}_{i,\delta}(0, j, 0) \mathbf{X}_i^0 \boldsymbol{\beta} + \left\{ \delta \sum_{s=1}^j \boldsymbol{\Psi}_{i,\delta}(0, j, s) \mathbf{X}_i(t_s) \boldsymbol{\gamma} \right\} \mathbf{1}_{\{j>0\}} \quad (10)$$

and

$$\begin{aligned} \mathbf{V}_{\Lambda_{ijj'}} &= \text{cov}\{\boldsymbol{\Lambda}_i(t_j); \boldsymbol{\Lambda}_i(t_{j'})\} \\ &= \boldsymbol{\Psi}_{i,\delta}(0, j, 0) \boldsymbol{\Psi}_{i,\delta}(0, j', 0)^\top \\ &\quad + \left[\boldsymbol{\Psi}_{i,\delta}(0, j, 0) \mathbf{B}_{uv} \left\{ \delta \sum_{s'=1}^{j'} \boldsymbol{\Psi}_{i,\delta}(0, j', s') \mathbf{Z}_i(t_{is'}) \right\}^\top \right] \mathbf{1}_{\{j>0\}} \\ &\quad + \left[\left\{ \delta \sum_{s=1}^j \boldsymbol{\Psi}_{i,\delta}(0, j, s) \mathbf{Z}_i(t_s) \right\} \mathbf{B}_{uv}^\top \boldsymbol{\Psi}_{i,\delta}(0, j', 0)^\top \right] \mathbf{1}_{\{j>0\}} \\ &\quad + \left[\left\{ \delta \sum_{s=1}^j \boldsymbol{\Psi}_{i,\delta}(0, j, s) \mathbf{Z}_i(t_s) \right\} \mathbf{B}_v \left\{ \delta \sum_{s'=1}^{j'} \boldsymbol{\Psi}_{i,\delta}(0, j', s') \mathbf{Z}_i(t_{is'}) \right\}^\top \right] \mathbf{1}_{\{\min(j,j')>0\}} \end{aligned} \quad (11)$$

It can be deduced that the vector of incomplete and transformed data $\tilde{\mathbf{Y}}_{ij}^*$ at occasion j is multivariate Gaussian with expectation $\boldsymbol{\mu}_{\tilde{\mathbf{Y}}_{ij}^*} = \mathbf{M}_{ij} \mathbf{P} \boldsymbol{\mu}_{\Lambda_{ij}}$ and variance-covariance matrix

$\mathbf{V}_{\tilde{\mathbf{Y}}_{ij}^*} = \mathbf{M}_{ij} (\mathbf{P} \mathbf{V}_{\Lambda_{ijj}} \mathbf{P}^\top + \boldsymbol{\Sigma}) \mathbf{M}_{ij}^\top$, and the total vector of incomplete and transformed data $\tilde{\mathbf{Y}}_i^* = (\tilde{\mathbf{Y}}_{ij}^{*\top})_{j \in \tau_i}^\top$ is multivariate Gaussian with expectation $\boldsymbol{\mu}_{\tilde{\mathbf{Y}}_i^*} = (\boldsymbol{\mu}_{\tilde{\mathbf{Y}}_{ij}^*}^\top)_{j \in \tau_i}^\top$ and variance-covariance matrix $\mathbf{V}_{\tilde{\mathbf{Y}}_i^*}$, a block matrix with $\mathbf{M}_{ij} \mathbf{P} \mathbf{V}_{\Lambda_{ijj'}} \mathbf{P}^\top \mathbf{M}_{ij'}^\top + (\mathbf{M}_{ij} \boldsymbol{\Sigma} \mathbf{M}_{ij'}^\top) \mathbf{1}_{\{j=j'\}}$ the (j, j') block.

3.3.2 Likelihood

As the N subjects of the sample are independent, the log-likelihood of the model is $L(Y^*; \boldsymbol{\theta}) = \sum_{i=1}^N \log \left\{ \mathcal{L}_i(\mathbf{Y}_i^*; \boldsymbol{\theta}) \right\}$ with $\mathcal{L}_i(\mathbf{Y}_i^*; \boldsymbol{\theta})$ the individual contribution to the likelihood. Here,

$\boldsymbol{\theta} = (\boldsymbol{\beta}^\top, \boldsymbol{\gamma}^\top, \text{vec}(\mathbf{L})^\top, (\boldsymbol{\alpha}_{dd'})_{d,d' \in \{1, \dots, D\}^2}, (\sigma_k)_{k \in \{1, \dots, K\}}, \boldsymbol{\eta}^\top)^\top$ is the whole vector of parameters. Using the Jacobian of the link functions H_k ($k = 1, \dots, K$), the individual contribution is:

$$\mathcal{L}_i(\mathbf{Y}_i^*; \boldsymbol{\theta}) = \phi_i(\tilde{\mathbf{Y}}_i^*; \boldsymbol{\mu}_{\tilde{\mathbf{Y}}_i^*}, \mathbf{V}_{\tilde{\mathbf{Y}}_i^*}) \prod_{j \in \tau_i} \prod_{l=1}^{K_{ij}^*} \mathcal{J}_{\kappa(l)} \left\{ H_{\kappa(l)}(\tilde{\mathbf{Y}}_{ij\kappa(l)}^*; \boldsymbol{\eta}_{\kappa(l)}) \right\} \quad (12)$$

where $\phi_i(\cdot; \boldsymbol{\mu}, \mathbf{V})$ denotes the density function of a multivariate Gaussian vector with expectation $\boldsymbol{\mu}$ and variance-covariance \mathbf{V} , and $\mathcal{J}_{\kappa(l)} \left\{ H_{\kappa(l)}(\tilde{\mathbf{Y}}_{ij\kappa(l)}^*; \boldsymbol{\eta}_{\kappa(l)}) \right\}$ denotes the Jacobian of the link function

$H_{\kappa(l)}$ used to transform $Y_{ij\kappa(l)}^*$, the l^{th} observed marker at occasion j for subject i . For instance, with the linear link function defined in (2), $\mathcal{J}_{\kappa(l)}\left\{H_{\kappa(l)}(\tilde{Y}_{ij\kappa(l)}^*; \eta_{\kappa(l)})\right\} = \frac{1}{\eta_{\kappa(l)}}$.

3.3.3 Optimization Algorithm and Implementation

The maximum likelihood estimates are obtained using an extended Levenberg-Marquardt algorithm (Marquardt, 1963) because of its robustness and good convergence rate. At each iteration p , if necessary, the Hessian matrix $\mathbf{H}^{(p)}$ is diagonal-inflated to obtain a positive definite matrix $\mathbf{H}^{*(p)}$ which is used to update the parameters $\boldsymbol{\theta}^{(p+1)} = \boldsymbol{\theta}^{(p)} - \nu \left(\mathbf{H}^{*(p)}\right)^{-1} \mathbf{U}(\boldsymbol{\theta}^{(p)})$, with $\mathbf{U}(\boldsymbol{\theta}^{(p)})$ the gradient at iteration p and ν the improvement control parameter. Convergence is reached when $\|\boldsymbol{\theta}^{(p+1)} - \boldsymbol{\theta}^{(p)}\|_2 < \epsilon_\theta$, $|L(\mathbf{Y}^*; \boldsymbol{\theta}^{(p+1)}) - L(\mathbf{Y}^*; \boldsymbol{\theta}^{(p)})| < \epsilon_L$ and $\frac{\mathbf{U}(\boldsymbol{\theta}^{(p)})^\top (\mathbf{H}^{(p)})^{-1} \mathbf{U}(\boldsymbol{\theta}^{(p)})}{n_{\text{para}}} < \epsilon_H$, with n_{para} the total number of parameters. The latter criterion is by far the most stringent one and specifically targets maximum search so that $\epsilon_\theta = \epsilon_L = \epsilon_H = 10^{-3}$ is small enough to ensure convergence. The variances of the estimators are obtained from the inverse of $\mathbf{H}^{(p)}$.

Given the possibly high number of parameters, we first estimate the parameters for each process taken separately, then we start the maximization of the likelihood of the multivariate model from these simple estimates, setting initial values of the inter-dimension parameters to zero. The model estimation is implemented in R; it combines R and C_{++} languages, and includes parallel computations. The program is available for download at <https://github.com/bachirtadde/CInLPN>.

3.4 Marginal and subject-specific predictions

The goodness-of-fit of the model can be assessed by comparing predictions with observations of the markers in their transformed scales. From notations defined in Section 3.3.1, marginal and conditional distributions of the markers are:

$$\tilde{\mathbf{Y}}_i \sim \mathcal{N}\left(\mathbf{P}\boldsymbol{\mu}_{\Lambda_i}, \left(\mathbf{P}\mathbf{V}_{\Lambda_i}\mathbf{P}^\top + \boldsymbol{\Sigma}_i\right)\right). \quad (13)$$

$$\tilde{\mathbf{Y}}_i \Big|_{\Lambda_i} \sim \mathcal{N}\left(\mathbf{P}\boldsymbol{\Lambda}_i, \boldsymbol{\Sigma}_i\right) \quad (14)$$

where $\boldsymbol{\Sigma}_i$ is the block-diagonal matrix constituted of n_i $\boldsymbol{\Sigma}$ blocks.

The marginal ($\mathbf{Y}_i^{(M)}$) and subject-specific ($\mathbf{Y}_i^{(SS)}$) predictions in the transformed scales are then respectively obtained by taking the expectations of the marginal and conditional distributions of the transformed markers at the parameter estimates $\hat{\boldsymbol{\theta}}$ and at the predicted latent processes $\hat{\boldsymbol{\Lambda}}_i$ of $\boldsymbol{\Lambda}_i$ given the observations $\tilde{\mathbf{Y}}_i^*$: $\hat{\boldsymbol{\Lambda}}_i = E\left(\boldsymbol{\Lambda}_i \mid \tilde{\mathbf{Y}}_i^*\right) = \boldsymbol{\mu}_{\Lambda_i} + \mathbf{C}_{\Lambda_i \tilde{\mathbf{Y}}_i^*} \mathbf{V}_{\tilde{\mathbf{Y}}_i^*}^{-1} \left(\tilde{\mathbf{Y}}_i^* - \boldsymbol{\mu}_{\tilde{\mathbf{Y}}_i^*}\right)$, where $\mathbf{C}_{\Lambda_i \tilde{\mathbf{Y}}_i^*} = \left(\mathbf{V}_{\Lambda_{ijj'}} \mathbf{P}^\top \mathbf{M}_{ij'}^\top\right)_{(j,j') \in \tau^2}$ is the covariance matrix between $\boldsymbol{\Lambda}_i$ and $\tilde{\mathbf{Y}}_i^*$.

Using these individual predictions, one can graphically compare either the marginal predictions $\mathbf{Y}^{(M)}$ or subject-specific predictions $\mathbf{Y}^{(SS)}$ averaged within time intervals to the observations averaged

within the same time intervals. Marginal and subject-specific predictions in the natural scale of the markers can also be derived from the marginal and conditional distributions by using a Monte-Carlo approximation (Proust-Lima et al., 2013).

4 Simulations

We performed two series of simulations to evaluate the estimation program and the impact of time discretization on the interpretation of $\mathbf{A}_{i,\delta}(t)$ matrix.

4.1 Simulation Study 1: Validation of the estimation program

4.1.1 Design

To evaluate the estimation program, we generated a system of two Gaussian processes ($(\mathbf{\Lambda}^1(t_j))_{t_j \geq 0}$ and $(\mathbf{\Lambda}^2(t_j))_{t_j \geq 0}$), with $t_j = j \times \delta$, $j \in \{0, \dots, J\}$. Each process is measured by one longitudinal marker (\mathbf{Y}_1 and \mathbf{Y}_2 , respectively) and two covariates, one continuous C_1 and one binary C_2 . We considered two scenarios: a covariate-specific structure of temporal influences (Scenario 1) and a time-dependent temporal influences structure (Scenario 2). In Scenario 1, we assumed a constant rate of change for the system of latent processes (with random intercepts and simple effects of both covariates in the sub-models for the initial level and the change over time) and a structure of temporal influences $\mathbf{A}_{i,\delta}$ different for each level of C_1 :

$$\left\{ \begin{array}{l} \Lambda_i^1(0) = \beta_0^1 + \beta_1^1 C_{1,i} + \beta_2^1 C_{2,i} + u_i^1 \\ \Lambda_i^2(0) = \beta_0^2 + \beta_1^2 C_{1,i} + \beta_2^2 C_{2,i} + u_i^2 \\ \frac{\Delta \Lambda_i^1(t_j + \delta)}{\delta} = \gamma_0^1 + \gamma_1^1 C_{1,i} + \gamma_2^1 C_{2,i} + v_i^1 + (\alpha_{i,11}^0 + \alpha_{i,11}^1 C_{2,i}) \Lambda_i^1(t_j) + (\alpha_{i,12}^0 + \alpha_{i,12}^1 C_{2,i}) \Lambda_i^2(t_j) \\ \frac{\Delta \Lambda_i^2(t_j + \delta)}{\delta} = \gamma_0^2 + \gamma_1^2 C_{1,i} + \gamma_2^2 C_{2,i} + v_i^2 + (\alpha_{i,21}^0 + \alpha_{i,21}^1 C_{2,i}) \Lambda_i^1(t_j) + (\alpha_{i,22}^0 + \alpha_{i,22}^1 C_{2,i}) \Lambda_i^2(t_j) \\ \frac{Y_{ijk} - \eta_{0k}}{\eta_{1k}} = \Lambda_i^k(t_j) + \tilde{\epsilon}_{ijk}, \quad k = 1, 2 \end{array} \right. \quad (15)$$

where $\mathbf{u}_i = (u_i^1, u_i^2)^\top$, $\mathbf{v}_i = (v_i^1, v_i^2)^\top$ and $(\mathbf{u}_i^\top, \mathbf{v}_i^\top)^\top \sim \mathcal{N}(0, \mathbf{L}\mathbf{L}^\top)$ with \mathbf{L} such that the random effects are independent between dimensions, and $\tilde{\epsilon}_{ijk} \sim \mathcal{N}(0, \sigma_k^2)$, $\forall k \in \{1, 2\}$.

In scenario 2, we considered initial levels adjusted for the binary covariate C_2 , constant rates of change with no adjustment, and temporal influences between two processes $\mathbf{A}_{i,\delta}(t_j)$ that evolved with time:

$$\left\{ \begin{array}{l} \Lambda_i^1(0) = \beta_0^1 + \beta_1^1 C_{2,i} + u_i^1 \\ \Lambda_i^2(0) = \beta_0^2 + \beta_1^2 C_{2,i} + u_i^2 \\ \frac{\Delta \Lambda_i^1(t_j + \delta)}{\delta} = \gamma_0^1 + v_i^1 + a_{11}(t_j) \Lambda_i^1(t_j) + a_{12}(t_j) \Lambda_i^2(t_j) \\ \frac{\Delta \Lambda_i^2(t_j + \delta)}{\delta} = \gamma_0^2 + v_i^2 + a_{21}(t_j) \Lambda_i^1(t_j) + a_{22}(t_j) \Lambda_i^2(t_j) \\ \frac{Y_{ijk} - \eta_{0k}}{\eta_{1k}} = \Lambda_i^k(t_j) + \tilde{\epsilon}_{ijk}, \quad k = 1, 2, \end{array} \right. \quad (16)$$

where $\mathbf{u}_i = (u_i^1, u_i^2)^\top$, $\mathbf{v}_i = (v_i^1, v_i^2)^\top$ and $(\mathbf{u}_i^\top, \mathbf{v}_i^\top)^\top \sim \mathcal{N}(0, \mathbf{L}\mathbf{L}^\top)$ with \mathbf{L} such that the random effects are independent between dimensions, and $\tilde{\epsilon}_{ijk} \sim \mathcal{N}(0, \sigma_k^2)$, $\forall k \in \{1, 2\}$. Each element of the matrix of temporal influences $a_{kk'}(t)$ is defined from a basis of quadratic B-splines with one internal knot at the median $(\mathbf{S}_m)_{\{m=1,3\}}$ so that $a_{kk'}(t) = \alpha_{kk'}^0 + \alpha_{kk'}^1 \mathbf{S}_1(t) + \alpha_{kk'}^2 \mathbf{S}_2(t) + \alpha_{kk'}^3 \mathbf{S}_3(t)$, $\forall k \neq k'$ and $(k, k') \in \{1, 2\}^2$ (diagonal elements were not adjusted).

The design of the simulations and the parameters were chosen to mimic the ADNI data. Dimensions 1 and 2 were cerebral anatomy and cognitive ability, each one measured by a specific composite score. Covariate C_1 represented the baseline age centered on the mean age in decade and was generated according to a Gaussian distribution: $C_1 \sim \mathcal{N}(0, 0.64)$. Covariate C_2 corresponded to the indicator of group CN *versus* group MCI. It was generated according to a Bernoulli distribution with probability 0.37. We used a discretization step $\delta = 1$ (i.e., 6 months in ADNI 1 data). Markers observations were generated every 6 months up to 3 years. Thus a subject had 7 repeated measures at occasions $j \in \{0, 1, \dots, 6\}$. We also considered a design in which scheduled visits could be missed completely at random with a probability of 0.15, and when a visit was not missed, a marker could be missing with a probability of 0.07. For each design and scenario, we generated 1000 samples of 512 subjects.

4.1.2 Results

Web Table 1 of the Web Appendix B and Table 1 provide the results of the simulations for scenarios 1 and 2, respectively. In both settings, all the parameters were correctly estimated with satisfying coverage rates in the absence of missing data (left part) and in the presence of missing data (right part).

4.2 Simulation Study 2: Impact of the discretization step on the temporal influence structure between processes

4.2.1 Design

To formally assess whether the interpretation under the discretized time was the same as the one obtained under continuous time, we assessed the type-I error rate associated with each non diagonal element of the matrix of temporal influences \mathbf{A} under three discretization steps $\delta = 1/3$ (for 2 months), $1/2$ (for 3 months) and 1 (for 6 months) when data were actually generated under continuous time (approximated by a step $\delta=0.001$). We considered for this a system of three latent processes $((\mathbf{\Lambda}^1(t_j))_{t_j \geq 0}, (\mathbf{\Lambda}^2(t_j))_{t_j \geq 0}, \text{ and } (\mathbf{\Lambda}^3(t_j))_{t_j \geq 0})$, with $t_j = j \times \delta$, $\delta = 0.001$. Each process is measured by one Gaussian repeated marker $(\mathbf{Y}_1, \mathbf{Y}_2, \mathbf{Y}_3)$. The processes have constant rate of change, with no

Table 1: Results of the simulations for scenario 2 (1000 replicates of samples of size 512).

	without missing values						with missing values*				
	θ	$\hat{\theta}$	bias [†]	ESE [‡]	ASE [‡]	CR(%)	$\hat{\theta}$	bias	ESE [‡]	ASE [‡]	CR(%)
β_1^1	-1.635	-1.644	0.5	0.109	0.108	95.5	-1.644	0.5	0.109	0.109	94.7
β_1^2	-1.784	-1.789	0.2	0.115	0.119	95.7	-1.790	0.3	0.119	0.121	94.8
γ_0^1	0.009	0.009	1.4	0.009	0.009	96.0	0.009	1.6	0.009	0.010	95.5
γ_0^2	-0.053	-0.053	1.5	0.017	0.017	95.5	-0.053	1.3	0.017	0.018	95.6
L(3,1)	0.032	0.031	3.2	0.009	0.010	95.2	0.031	3.2	0.010	0.010	95.5
L(4,2)	-0.011	-0.009	19.5	0.014	0.015	95.4	-0.009	20.5	0.014	0.015	94.7
L(3,3)	0.094	0.094	0.1	0.006	0.006	94.6	0.094	0.3	0.006	0.006	93.9
L(4,4)	0.169	0.169	0.2	0.010	0.011	95.0	0.169	0.1	0.011	0.011	94.7
α_{11}^0	-0.012	-0.011	8.2	0.008	0.009	95.3	-0.011	8.3	0.009	0.009	95.6
α_{12}^0	0.115	0.114	0.9	0.018	0.018	93.8	0.113	1.1	0.020	0.020	94.9
α_{12}^1	-0.092	-0.092	0.3	0.027	0.027	94.9	-0.092	0.6	0.030	0.030	96.4
α_{12}^2	-0.028	-0.028	3.2	0.015	0.015	94.5	-0.027	4.1	0.017	0.017	95.1
α_{12}^3	-0.069	-0.069	0.1	0.026	0.026	94.1	-0.069	0.2	0.028	0.029	95.1
α_{21}^0	0.134	0.135	0.7	0.033	0.034	94.2	0.135	0.4	0.036	0.036	94.8
α_{21}^1	-0.076	-0.075	0.9	0.052	0.052	93.6	-0.075	1.2	0.058	0.058	94.5
α_{21}^2	0.024	0.022	11.3	0.031	0.035	95.4	0.023	7.9	0.034	0.034	95.4
α_{21}^3	-0.140	-0.130	6.8	0.052	0.052	94.2	-0.130	7.0	0.058	0.058	94.0
α_{22}^0	0.009	0.007	22.2	0.012	0.012	94.8	0.007	21.6	0.013	0.013	94.7
σ_1	0.376	0.378	0.5	0.013	0.013	94.9	0.378	0.5	0.013	0.013	95.2
σ_2	0.686	0.688	0.2	0.027	0.026	93.9	0.688	0.3	0.028	0.027	93.6
η_{01}	3.878	3.886	0.2	0.196	0.198	95.1	3.885	0.2	0.196	0.199	94.8
η_{11}	2.678	2.667	0.4	0.087	0.087	95.1	2.667	0.4	0.088	0.088	94.9
η_{02}	2.589	2.591	0.1	0.112	0.114	95.9	2.591	0.1	0.114	0.115	95.3
η_{12}	1.472	1.470	0.1	0.054	0.052	93.5	1.470	0.2	0.056	0.054	93.4

* (15% missing occasions, 7% missing outcomes),

† relative bias(%),

‡ ASE is the asymptotic standard error, ESE is the empirical standard error and CR is the coverage rate of the 95% confidence interval,

diagonal elements of the temporal influences matrix were not adjusted for time.

adjustment for covariates and a matrix of temporal influences \mathbf{A} constant over time:

$$\left\{ \begin{array}{l} \Lambda_i^1(0) = \beta_0^1 + u_i^1 \\ \Lambda_i^2(0) = \beta_0^2 + u_i^2 \\ \Lambda_i^3(0) = \beta_0^3 + u_i^3 \\ \frac{\Delta\Lambda_i^1(t_j+\delta)}{\delta} = \gamma_0^1 + v_i^1 + a_{11}\Lambda_i^1(t_j) + a_{12}\Lambda_i^2(t_j) + a_{13}\Lambda_i^3(t_j) \\ \frac{\Delta\Lambda_i^2(t_j+\delta)}{\delta} = \gamma_0^2 + v_i^2 + a_{21}\Lambda_i^1(t_j) + a_{22}\Lambda_i^2(t_j) + a_{23}\Lambda_i^3(t_j) \\ \frac{\Delta\Lambda_i^3(t_j+\delta)}{\delta} = \gamma_0^3 + v_i^3 + a_{31}\Lambda_i^1(t_j) + a_{32}\Lambda_i^2(t_j) + a_{33}\Lambda_i^3(t_j) \\ \frac{Y_{ijk} - \eta_{0k}}{\eta_{1k}} = \Lambda_i^k(t_j) + \tilde{\epsilon}_{ijk}, \quad k = 1, 2, 3 \end{array} \right. \quad (17)$$

The simulation model mimicked the ADNI data with cerebral anatomy, cognitive ability and functional autonomy as dimensions, respectively measured by a specific composite score. We estimated the model on the ADNI data with $\delta=1$ (6 months) and transformed the parameters to the scale $\delta=0.001$ to generate the data in almost continuous time. We provide in the Web Appendix A the formulas to relate model components defined under $\delta=1$ and $\delta=0.001$. Elements of the matrix of temporal influences were set one by one to 0 in $\delta = 0.001$ scale to evaluate the associated type-I error rate. Latent processes were generated with solver from dsolve package (Soetaert et al., 2010) and observations were derived every 6 months up to 3 years. We considered each time 1000 samples of 512 subjects.

4.2.2 Results

Table 2 displays the type-I error rates (in percentage) associated with each non diagonal element of the matrix of temporal influences \mathbf{A} when estimated with discretization steps $\delta=1/3, 1/2$ and 1. All the type-I error rates are close to the nominal 5% rate (95% interval of expected rates of [3.6, 6.4] with 1000 replicates). We note however that with a discretization step of $\delta=1$, the type-I error rates begin to somewhat increase, suggesting that with larger discretization steps, causal interpretations are altered.

5 Application

Using the ADNI data (Section 2), the application aimed to describe the decline over time of cerebral anatomy, cognitive ability and functional autonomy in three clinical stages of AD (normal aging (CN), Mild Cognitive Impairment (MCI) and diagnosed with Alzheimer’s Disease (dAD)) and to quantify the temporal influences between these dimensions by assessing especially whether the relationships differ according to the clinical stage. The dynamic model applied on ADNI is summarized in Figure 1.

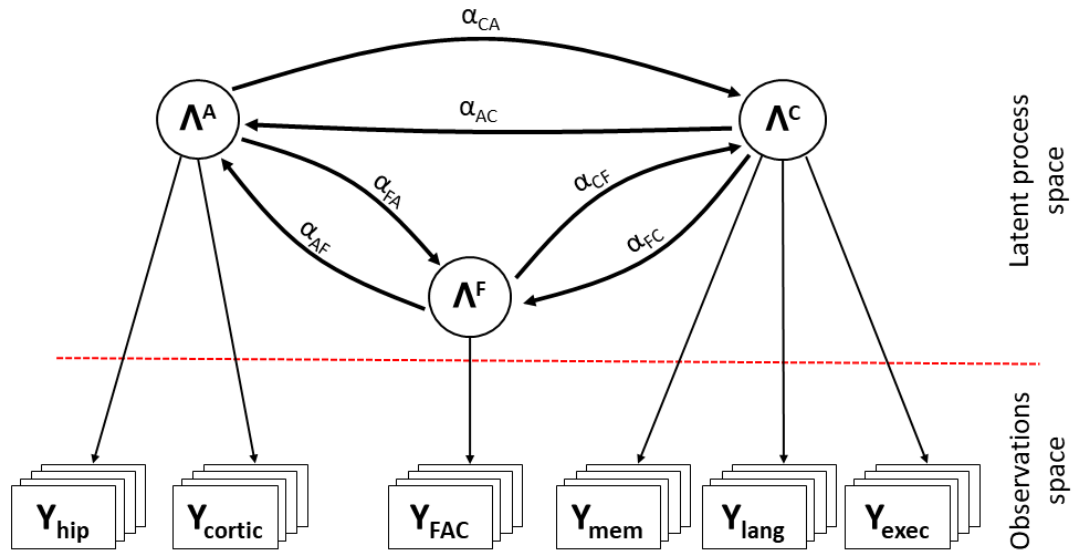


Figure 1: Graph of the dynamic causal model considered on ADNI 1 data with three dimensions (labelled Λ^A for cerebral anatomy, Λ^C for cognitive ability and Λ^F for functional autonomy). Cerebral anatomy is measured by two repeated volumes (Y_{hip} and Y_{cortic} for hippocampal volume and mean regional cortical thickness, respectively), cognitive ability by three repeated scores (Y_{mem} , Y_{lang} and Y_{exec} for sumscores in memory, language and executive functions, respectively) and functional autonomy by one repeated score (Y_{FAQ} for FAQ scale).

5.1 Measures and ADNI sample description

Cerebral anatomy ($\mathbf{\Lambda}^A$) was defined as the process underlying the hippocampal volume relative to total intracranial volume and the mean cortical thickness of nine regions (Freesurfer version 4.4.0 for longitudinal data) previously identified in a cortical signature of AD (Dickerson et al., 2008). Global cognitive ability ($\mathbf{\Lambda}^C$) was defined as the process underlying three cognitive markers of memory, language and executive functioning, respectively. Each marker was a composite score previously identified from the psychometric tests available in ADNI (Park et al., 2012). Functional autonomy ($\mathbf{\Lambda}^F$) was defined as the process underlying the observed sumscore of the FAQ (Functional Assessment Questionnaire) composed of 30 items (Pfeffer et al., 1982). Covariates were the age at entry (centered around 75.4 and indicated in decades), gender, educational level (low level if ≤ 12 years *vs* high level if >12 years), the APOE genotype ($\epsilon 4$ carrier *vs* $\epsilon 4$ non-carrier) and the 3 clinical stages (CN, MCI, dAD) as defined at inclusion in ADNI (we did not consider possible changes in stages during follow-up). We selected in the sample all the subjects who had no missing data for the covariates and had at least one observation for each dimension during the follow-up. The main analysis included 656 subjects (82% of the initial sample). The sample consisted of 190 (29%) subjects at healthy stage (CN), 322 (49%) subjects at mild cognitive impairment stage (MCI), and 144 (22%) subjects diagnosed with Alzheimer’s disease (dAD); 43% were females, 83% had a high educational level and 49% carried APOE $\epsilon 4$ allele. The mean age at entry was 75.4 years old (sd=6.6). The mean number of visits was 5, 6 and 4 for CN, MCI and dAD subjects, respectively.

5.2 Specification of the dynamic multivariate model

The initial levels of the processes were adjusted for gender, education, APOE genotype, clinical stage, and age at baseline. Changes of the processes over time were adjusted for gender, education, APOE genotype, clinical stage. In order to account for the correlations between individual repeated measures, we included random intercepts on the initial levels of the processes (correlated between processes) and random intercepts on the changes of the processes over time (independent between processes). The matrix of temporal influences that captured the interrelations between processes was constant over time and adjusted for clinical stage: $a_{dd'} = \alpha_{dd'}^0 + MCI \times \alpha_{dd'}^1 + dAD \times \alpha_{dd'}^2$, for $(d, d') \in \{A, C, F\}^2$. To correct the possible departure from normality of each observed marker, we transformed them using integrated quadratic splines (as in equation (4)) with 2 internal knots at the terciles for scores measuring cerebral and cognitive dimensions and with one internal knot at the median for the functional score.

In the main analysis, we considered a discretization step of approximately 3 months ($\delta = 0.23$ year) although observations were sparser as scheduled every 6 months. The modelling strategy consisted in finding first the best adjustment for each process taken separately with a significance threshold for covariate effects at 25%. Then, the whole multivariate model was estimated. In secondary analyses,

we re-estimated the final model by considering a discretization step of 1.5 months ($\delta = 0.125$ year) in order to evaluate whether the interpretations varied with a smaller step.

5.3 Results

5.3.1 Latent process-specific trajectories

Estimates of fixed effects, Cholesky’s decomposition parameters (for the random effects variance-covariance matrix) and measurement model parameters are provided in Web Tables 2, 3 and 4 of the Web Appendix C. In summary, older age, male gender, APOE $\epsilon 4$ carrying, and clinical stages MCI and dAD were associated with lower cerebral anatomy and lower cognitive ability levels at baseline. Higher education was associated with lower cerebral anatomy level but associated with higher cognitive ability level at baseline. Only clinical stages MCI and dAD were associated with lower functional autonomy level at baseline. Adjusted for other dimension levels, APOE $\epsilon 4$ carrying was associated with steeper declines in cerebral anatomy, cognitive ability and functional autonomy; and higher education was associated with steeper cerebral anatomy decline and smaller cognitive ability decline. Web Figure 1 of the Web Appendix C depicts the expected trajectories of each dimension according to stage for two profiles of individuals (women noncarrier of APOE $\epsilon 4$ and with lower educational level; men carrier of APOE $\epsilon 4$ and with higher educational level).

5.3.2 Temporal influence structure between processes

Estimates of the matrix of temporal influences are given in Table 3 and summarized in Figure 2 according to stage. Figure 2 shows that the temporal influences between cerebral anatomy ($\mathbf{\Lambda}^A$), cognitive ability ($\mathbf{\Lambda}^C$), and functional autonomy ($\mathbf{\Lambda}^F$) evolve from healthy stage to Alzheimer’s disease stage. At normal stage, cerebral dimension affects significantly the change of cognitive and functional dimensions while cognitive and functional dimensions tend to have reciprocal temporal dependencies. From MCI stage, the three dimensions become strongly interdependent with cognition as the central point: reciprocal temporal relationships appear between the anatomical and cognitive dimensions in addition to those between the functional and cognitive dimensions. At the dAD stage, the influence of the cerebral anatomy on functional autonomy and the effect of functional dimension (probably through its social component) on the cognitive dimension are attenuated and no more significant.

When considering a discretization step 1.5 months instead of 3 months, the Akaike Information criterion did not substantially differ ($AIC = 29550.5$ with 3 months and $AIC = 29547.1$ with 1.5 months) and the results regarding the temporal influence relationships remained the same (see Web Table 5 of the Web Appendix C).

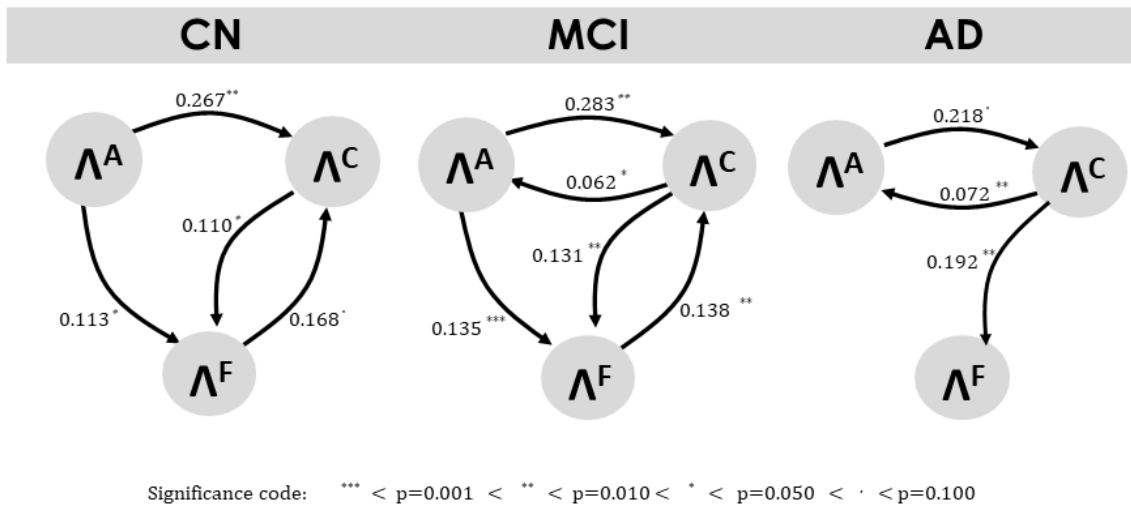


Figure 2: Temporal relationships estimated between cerebral anatomy (Λ^A), cognitive ability (Λ^C), and functional autonomy (Λ^F) at healthy (CN), MCI and dAD stages. Arrows represent effects of one dimension on the change of another dimension. Only the effects identified from Table 3 with a significance level lower than 10% are reported: numbers indicate the estimate and stars indicate the level of significance according to the Wald test.

5.3.3 Goodness-of-fit of the model

We assessed the goodness-of-fit of the model by comparing the subject-specific predictions with the observations of the markers in their transformed scale. On the original data, the predictions and observations, summarized by protocol visits and displayed in Figure 3, were very close showing the good fit of the model.

We also used a 5-fold cross-validation technique to avoid overoptimism in the predictions. Specifically, we split the sample into five groups (each one containing 20% of the subjects), and estimated the model using data from each combination of 4 groups and computed the subject-specific predictions on the remaining group. The predicted *versus* observed trajectories obtained on the 5 remaining groups, displayed in the Figure 3 of the Web Appendix C, confirmed the good fit of the model to the data.

6 Discussion

We proposed an original dynamic model to simultaneously describe multivariate processes over time and retrieve temporal relationships between the processes involved. Our model aims to be a dynamic causal model except that we relied on discrete time with difference equations (rather than continuous time with differential equations) to largely reduce the numerical problems, notably with a closed-form likelihood.

This approach goes further in the evaluation of temporal relationships compared to existing approaches such as DBN or CLM which quantify temporal associations by focusing on the effect of a system on the subsequent level of the system at the next visit. Two major differences are:

1. we work at a latent process level to avoid biases in association estimates due to the measurement error and to avoid the necessity to rely on complete and/or balanced observations. The importance of assessing associations at a latent process (or "true" error-free marker) level has been widely documented in a related context: the association between a longitudinal marker and a time-to-event (Rizopoulos, 2012).
2. we assess temporal relationships on the change of processes rather than the state of the system at a subsequent time. We can thus seek local dependence structures in line with the dynamic approach to causality. Yet we acknowledge that causal interpretation still has to be made cautiously as it is always subject to a correct specification of the statistical model.

One major simplifying assumption is the time discretization. Fundamentally, causal relationships are to be explored at an infinitesimal level and thus, a causal model is to be defined in continuous time (Commenges and Gégout-Petit, 2009; Aalen et al., 2016). However, in contrast with DBN and CLM discrete approaches, our discretization does not correspond to the visit process; it can be as precise as necessary. It only aims to avoid the numerical complexities due to differential equation modelling and

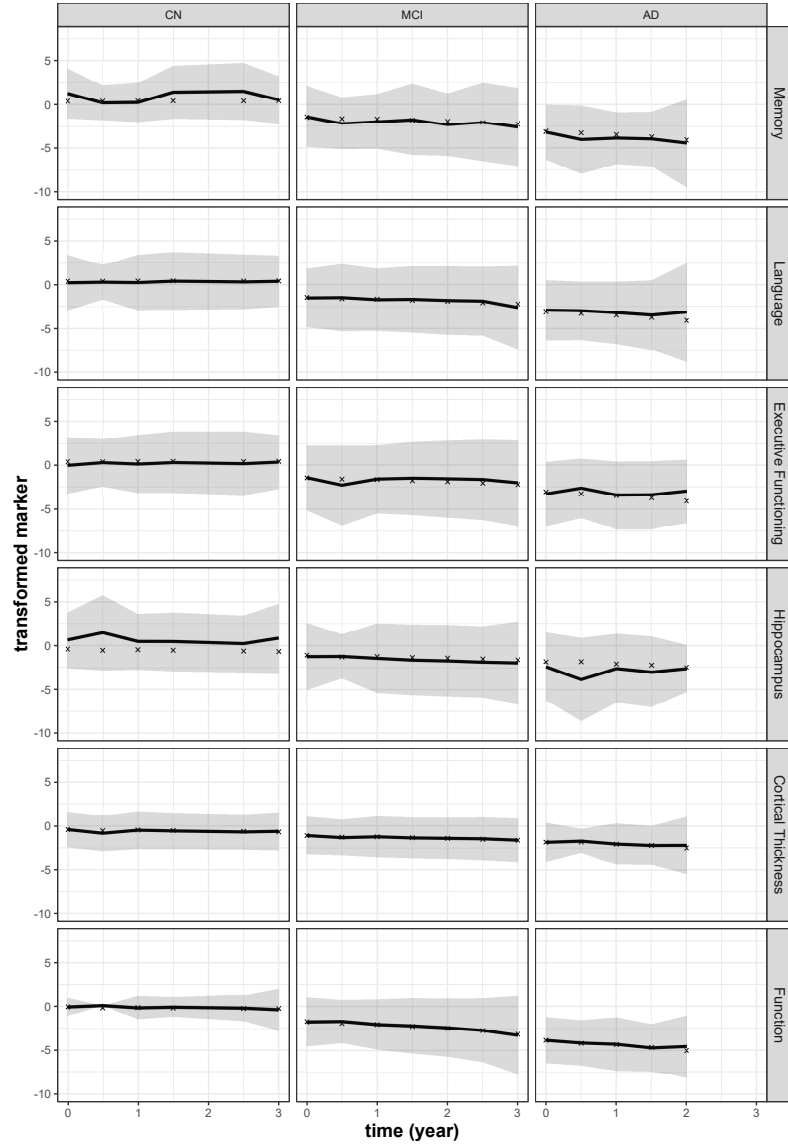


Figure 3: Mean transformed observed scores (plain lines) along with their 95% confidence interval (shadows) and corresponding mean subject-specific predictions (crosses) by protocol visit. Columns refer to the group (controls CN, subjects with Mild Cognitive Impairments MCI and subjects diagnosed with Alzheimer’s disease dAD). Rows refer to the markers (e.g., memory score, language score, executive functioning score, mean hippocampal volume, mean regional cortical thickness and FAQ score) in their transformed scales (see Web Figure 3 for the plot of the estimated link functions between the natural scale and the transformed scale).

provide a sensible understanding of the rate of change which is modelled. We assessed in a simulation study the impact of the discretization on the underlying time-continuous causal structure; we found that the type-I error rates of the temporal influence parameters were not altered by the use of a model in discrete time, provided the discretization step remained small in regards with the dynamics of the disease under study. Indeed in our simulations and application on Alzheimer’s disease, our discretization step was between 1.5 and 6 months while the disease progresses over decades (Amieva et al., 2008; Jack et al., 2013). In addition to this numerical assessment, we provided in supplementary material analytic approximate relationships between matrices of temporal influences defined in two discretization steps or in continuous and discrete time. In practice, we recommend to try several reasonable discretization steps, assess the change in goodness-of-fit and stability of the estimates, and retain the most sensible discretization step as a compromise between fit/stability and computational intensity.

Although presented in two parts, our structural model belongs to the family of nonlinear mixed models with specific mean and covariance structures which enable the estimation of temporal associations. Thus our estimation by maximum likelihood benefits from the same properties as mixed models. In particular, it handles imbalanced data and relies on the assumption that missing data (intermittent and monotone) are missing at random. This is realistic in ADNI 1 with its very short follow-up (3 years max). However, in applications with a longer follow-up, and notably in population-based cohorts, it will be probably necessary to account for informative clinical events, such as dementia and death in our context. In addition, in studies with a long follow-up, it may be reasonable to assume that the structure of temporal influences evolves with time. Our model can handle this as shown in the simulations.

The model was primarily motivated by the study of the multiple alterations involved in the dementia process in the elderly. Although there is a global agreement on the relevant dimensions in AD, their relationships are still poorly understood and a confusion persists between alterations due to normal aging and alterations due to pathological aging leading to dementia. Thanks to the ADNI data which included subjects at different clinical stages of dementia, we were able to exhibit the global structure of dependences between cerebral, cognitive and functional domains in normal aging. We found out that the main evolution in this structure due to the pathological process towards dementia (in subjects with mild cognitive impairment or diagnosed with AD) was on cognitive functioning with some effect of cognitive functioning on change in cerebral structure in addition to its effect on change in functional structure. This application which gives a first insight on the possibilities of this dynamic model, could be now refined by targeting specific brain regions (separating for instance cortical thicknesses from hippocampal volume) and specific cognitive functions (separating for instance memory from executive functioning).

As a conclusion, we proposed here a new methodology that may help identify temporal structures in

multivariate longitudinal data. Although applied in dementia context, this approach has potential to address unsolved questions in many other chronic diseases where multiple processes and/or markers are in play. This is the case in other neurodegenerative diseases (e.g., Parkinson, Multi-System Atrophy, Amyotrophic Lateral Sclerosis) but also beyond, for instance in chronic renal disease. The methodology could also help understand how dynamic exposures relate with markers of disease progression and disentangle in particular the direction of temporal associations when reverse causation (i.e., changes in the exposure due to early disease changes) may intervene.

Acknowledgements

This work benefited from the support of the project SMALA (ANR-15-CE37-0002) of the French National Research Agency (ANR). Computer time was provided by the computing facilities MCIA (Mésocentre de Calcul Intensif Aquitain) at the Université de Bordeaux and the Université de Pau et des Pays de l'Adour. Data collection and sharing for this project was funded by the Alzheimer's Disease Neuroimaging Initiative (ADNI) (National Institutes of Health Grant U01 AG024904) and DOD ADNI (Department of Defense award number W81XWH-12-2-0012).

References

- Aalen, O., Røysland, K., Gran, J., Kouyos, R., and Lange, T. (2016). Can we believe the DAGs? a comment on the relationship between causal DAGs and mechanisms. *Statistical methods in medical research* **25**, 2294–2314.
- Aalen, O. O. and Frigessi, A. (2007). What can statistics contribute to a causal understanding? *Scandinavian Journal of Statistics* **34**, 155–168.
- Amieva, H., Le Goff, M., Millet, X., Orgogozo, J. M., Pérès, K., Barberger-Gateau, P., Jacqmin-Gadda, H., and Dartigues, J. F. (2008). Prodromal Alzheimer's disease: successive emergence of the clinical symptoms. *Annals of neurology* **64**, 492–498.
- Commenges, D. and Gégout-Petit, A. (2009). A General Dynamical Statistical Model with Causal Interpretation. *Journal of the Royal Statistical Society. Series B (Statistical Methodology)* **71**, 719–736.
- Dickerson, B. C., Bakkour, A., Salat, D. H., Feczko, E., Pacheco, J., Greve, D. N., Grodstein, F., Wright, C. I., Blacker, D., Rosas, H. D., et al. (2008). The cortical signature of Alzheimer's disease: regionally specific cortical thinning relates to symptom severity in very mild to mild ad dementia and is detectable in asymptomatic amyloid-positive individuals. *Cerebral cortex* **19**, 497–510.

- Didelez, V. (2008). Graphical models for marked point processes based on local independence. *Journal of the Royal Statistical Society: Series B (Statistical Methodology)* **70**, 245–264.
- Donohue, M. C., Jacqmin-Gadda, H., Le Goff, M., Thomas, R. G., Raman, R., Gamst, A. C., and Beckett, L. A. (2014). Estimating long-term multivariate progression from short-term data. *Alzheimer’s & Dementia: The Journal of the Alzheimer’s Association* **10**, S400–410.
- Greenland, S. (2000). Causal Analysis in the Health Sciences. *Journal of the American Statistical Association* **95**, 286–289.
- Hamaker, E. L., Kuiper, R. M., and Grasman, R. P. (2015). A critique of the cross-lagged panel model. *Psychological methods* **20**, 102.
- Han, S. D., Gruhl, J., Beckett, L., Dodge, H. H., and Stricker, N. H. (2012). Beta amyloid, tau, neuroimaging, and cognition: sequence modeling of biomarkers for alzheimer’s disease. *Brain imaging and behavior* **6**, 610–620.
- Jack, C. R., Knopman, D. S., Jagust, W. J., Petersen, R. C., Weiner, M. W., Aisen, P. S., Shaw, L. M., Vemuri, P., Wiste, H. J., Weigand, S. D., et al. (2013). Tracking pathophysiological processes in Alzheimer’s disease: an updated hypothetical model of dynamic biomarkers. *The Lancet Neurology* **12**, 207–216.
- Kuiper, R. M. and Ryan, O. (2018). Drawing conclusions from cross-lagged relationships: Reconsidering the role of the time-interval. *Structural Equation Modeling: A Multidisciplinary Journal* pages 1–15.
- Landau, S. M., Harvey, D., Madison, C. M., Koeppe, R. A., Reiman, E. M., Foster, N. L., Weiner, M. W., and Jagust, W. J. (2011). Associations between cognitive, functional, and FDG-PET measures of decline in AD and MCI. *Neurobiology of Aging* **32**, 1207 – 1218.
- Marquardt, D. W. (1963). An algorithm for least-squares estimation of nonlinear parameters. *Journal of the society for Industrial and Applied Mathematics* **11**, 431–441.
- Mueller, S. G., Weiner, M. W., Thal, L. J., Petersen, R. C., Jack, C., Jagust, W., Trojanowski, J. Q., Toga, A. W., and Beckett, L. (2005). The Alzheimer’s disease Neuroimaging Initiative. *Neuroimaging Clinics of North America* **15**, 869–877.
- Mungas, D., Harvey, D., Reed, B., Jagust, W., DeCarli, C., Beckett, L., Mack, W., Kramer, J., Weiner, M., Schuff, N., et al. (2005). Longitudinal volumetric MRI change and rate of cognitive decline. *Neurology* **65**, 565–571.

- Park, L. Q., Gross, A. L., McLaren, D. G., Pa, J., Johnson, J. K., Mitchell, M., Manly, J. J., and Alzheimer’s Disease Neuroimaging Initiative (2012). Confirmatory factor analysis of the ADNI Neuropsychological Battery. *Brain Imaging and Behavior* **6**, 528–539.
- Pfeffer, R. I., Kurosaki, T. T., Harrah, C. H., Chance, J. M., and Filos, S. (1982). Measurement of functional activities in older adults in the community. *Journal of Gerontology* **37**, 323–329.
- Prague, M., Commenges, D., Gran, J., Ledergerber, B., Young, J., Furrer, H., and Thiebaut, R. (2017). Dynamic models for estimating the effect of HAART on CD4 in observational studies: application to the Aquitaine Cohort and the Swiss HIV Cohort Study. *Biometrics* **73**, 294–304.
- Proust-Lima, C., Amieva, H., and Jacqmin-Gadda, H. (2013). Analysis of multivariate mixed longitudinal data: a flexible latent process approach. *British Journal of Mathematical and Statistical Psychology* **66**, 470–487.
- Ramsay, J. O. (1988). Monotone regression splines in action. *Statistical Science* **3**, 425–441.
- Reitz, C. and Mayeux, R. (2014). Alzheimer’s disease: epidemiology, diagnostic criteria, risk factors and biomarkers. *Biochemical pharmacology* **88**, 640–651.
- Rizopoulos, D. (2012). *Joint models for longitudinal and time-to-event data with applications in R*. CRC Biostatistics Series 6. CRC Press, Boca Raton.
- Robitaille, A., Muniz, G., Piccinin, A. M., Johansson, B., and Hofer, S. M. (2012). Multivariate longitudinal modeling of cognitive aging: Associations among change and variation in processing speed and visuospatial ability. *GeroPsych: The Journal of Gerontopsychology and Geriatric Psychiatry* **25**, 15.
- Soetaert, K., Petzoldt, T., and Setzer, R. W. (2010). Solving differential equations in r: Package *deSolve*. *Journal of Statistical Software* **33**, 1–25.
- Song, L., Kolar, M., and Xing, E. P. (2009). Time-varying dynamic bayesian networks. In *Advances in Neural Information Processing Systems*, pages 1732–1740.
- Voelkle, M. C., Gische, C., Driver, C. C., and Lindenberger, U. (2018). The Role of Time in the Quest for Understanding Psychological Mechanisms. *Multivariate Behavioral Research* **53**, 782–805.
- Wimo, A., Guerchet, M., Ali, G.-C., Wu, Y.-T., Prina, A. M., Winblad, B., Jönsson, L., Liu, Z., and Prince, M. (2017). The worldwide costs of dementia 2015 and comparisons with 2010. *Alzheimer’s & Dementia* **13**, 1–7.

Appendix A: Relationships between model components under different discretization steps

For computational reasons, the latent processes in the structural model are assumed to evolve in discrete time with a constant step δ which may vary depending on the application. In reality the processes evolve in continuous time and causal inference should be done in continuous time. We thus established the relationship between transition matrices obtained under different discretization steps: δ^* and a smaller discretization step δ with $\delta^* = \rho \times \delta$ and integer $\rho > 1$.

With a discretization step $\delta = \frac{\delta^*}{\rho}$, the second line of equation (1) in the main paper can be rewritten:

$$\mathbf{\Lambda}_i(t + \delta) = \delta (\mathbf{X}_i(t + \delta)\boldsymbol{\gamma} + \mathbf{Z}_i(t + \delta)\mathbf{v}_i) + (\mathbf{I}_D + \delta\mathbf{A}_{i,\delta}(t)) \mathbf{\Lambda}_i(t), \quad \forall t > 0, \rho > 1 \quad (18)$$

By recurrence, the network level at $t + \rho\delta$, that also correspond to $t + \delta^*$, can be expressed as a function of $\mathbf{\Lambda}_i(t + \delta^*)$ as follows:

$$\mathbf{\Lambda}_i(t + \delta^*) = \boldsymbol{\Psi}_{i,\delta}(t, \rho, 0)\mathbf{\Lambda}_i(t) + \delta \sum_{s=1}^{\rho} \boldsymbol{\Psi}_{i,\delta}(t, \rho, s) (\mathbf{X}_i(t + \delta s)\boldsymbol{\gamma} + \mathbf{Z}_i(t + \delta s)\mathbf{v}_i) \quad (19)$$

with function $\boldsymbol{\Psi}_{i,\delta}$ defined in the relation (7) of the main paper.

Considering directly a discretization step of δ^* , the second line of equation (1) of the main paper can also be rewritten

$$\mathbf{\Lambda}_i(t + \delta^*) = \delta^* (\mathbf{X}_i(t + \delta^*)\boldsymbol{\gamma}^* + \mathbf{Z}_i(t + \delta^*)\mathbf{v}_i^*) + (\mathbf{I}_D + \delta^*\mathbf{A}_{i,\delta^*}(t)) \mathbf{\Lambda}_i(t), \quad \forall t > 0 \quad \text{and} \quad \delta^* > 0. \quad (20)$$

Relationships between transition matrices under different steps Considering that the second parts of equations (19) and (20) are close enough although the model specifications are different, we obtain:

$$\mathbf{I}_D + \delta^*\mathbf{A}_{i,\delta^*}(t) \approx \boldsymbol{\Psi}_{i,\delta}(t, \rho, 0) = \prod_{l=0}^{\rho-1} \left(\mathbf{I}_D + \frac{\delta^*}{\rho} \mathbf{A}_{i,\delta}(t + l\frac{\delta^*}{\rho}) \right) \quad (21)$$

Equation (21) can be rewritten to highlight the relationship between the causal structure \mathbf{A}_{i,δ^*} and $\mathbf{A}_{i,\delta}$:

$$\mathbf{A}_{i,\delta^*}(t) = \frac{1}{\delta^*} \left(\prod_{l=0}^{\rho-1} \left(\mathbf{I}_D + \frac{\delta^*}{\rho} \mathbf{A}_{i,\delta}(t + l\frac{\delta^*}{\rho}) \right) - \mathbf{I}_D \right) \quad (22)$$

When assuming that the causal structure $\mathbf{A}_{i,\delta}$ is constant in each interval $[t, t + \delta^*]$, $\forall t \in \tau$, the relationship (22) becomes :

$$\mathbf{A}_{i,\delta^*}(t) = \frac{1}{\delta^*} \left(\left(\mathbf{I}_D + \frac{\delta^*}{\rho} \mathbf{A}_{i,\delta}(t) \right)^\rho - \mathbf{I}_D \right) \quad (23)$$

Or equivalently,

$$\mathbf{A}_{i,\delta}(t) = \frac{\rho}{(\delta^*)^{(\rho+1)}} \left(\left(\frac{1}{\delta^*} \mathbf{I}_D + \mathbf{A}_{i,\delta^*}(t) \right)^{\frac{1}{\rho}} - \mathbf{I}_D \right) \quad (24)$$

Note that the limits of the right part of relation (23), when ρ tends to infinity provide the relationship between $\mathbf{A}_{i,\delta^*}(t)$ and its continuous time counterpart. Assuming that $\lim_{\rho \rightarrow \infty} \mathbf{A}_{i,\delta}(t) = \mathbf{A}_i(t)$ is finite, the relationship (23), become:

$$\mathbf{A}_{i,\delta^*}(t) \approx \frac{1}{\delta^*} (\exp(\delta^* \mathbf{A}_i(t)) - \mathbf{I}_D) \quad (25)$$

Relationships between trend parameters under different steps To relate the transition matrices under different steps, we considered second parts of equations (19) and (20) were close enough. We identified:

$$\begin{cases} \mathbf{X}_i(t + \delta^*) \boldsymbol{\gamma}^* \approx \frac{1}{\rho} \sum_{s=1}^{\rho} \boldsymbol{\Psi}_{i,\delta}(t, \rho, s) \mathbf{X}_i(t + \frac{\delta^*}{\rho} s) \boldsymbol{\gamma} \\ \mathbf{Z}_i(t + \delta^*) \mathbf{v}_i^* \approx \frac{1}{\rho} \sum_{s=1}^{\rho} \boldsymbol{\Psi}_{i,\delta}(t, \rho, s) \mathbf{Z}_i(t + \frac{\delta^*}{\rho} s) \mathbf{v}_i \end{cases} \quad (26)$$

In the particular case where \mathbf{X}_i and \mathbf{Z}_i reduce to intercepts,

$$\begin{cases} \gamma^* \approx \frac{1}{\rho} \sum_{s=1}^{\rho} \boldsymbol{\Psi}_{i,\delta}(t, \rho, s) \gamma \\ \mathbf{v}_i^* \approx \frac{1}{\rho} \sum_{s=1}^{\rho} \boldsymbol{\Psi}_{i,\delta}(t, \rho, s) \mathbf{v}_i \end{cases} \quad (27)$$

Or equivalently,

$$\begin{cases} \gamma \approx \rho \left(\sum_{s=1}^{\rho} \boldsymbol{\Psi}_{i,\delta}(t, \rho, s) \right)^{-1} \gamma^* \\ \mathbf{v}_i \approx \rho \left(\sum_{s=1}^{\rho} \boldsymbol{\Psi}_{i,\delta}(t, \rho, s) \right)^{-1} \mathbf{v}_i^* \end{cases} \quad (28)$$

Appendix B: Additional results in the simulations studies

Table 4: Results of the simulations (1000 replicates of samples with 512 subjects) considering two latent processes, each one repeatedly measured by a marker, with linear trajectories and constant covariate-specific causal structure. ASE is the asymptotic standard error, ESE is the empirical standard error and CR is the coverage rate of the 95% confidence interval.

	without missing values						with missing values*				
	θ	$\hat{\theta}$	bias [†]	ESE [‡]	ASE [‡]	CR(%)	$\hat{\theta}$	bias	ESE [‡]	ASE [‡]	CR(%)
β_1^1	-0.268	-0.270	0.8	0.070	0.073	96.2	-0.271	1.0	0.072	0.074	95.5
β_2^1	-1.695	-1.704	0.5	0.113	0.111	94.3	-1.702	0.4	0.117	0.114	94.4
β_1^2	0.057	0.059	4.0	0.082	0.085	92.3	0.056	1.1	0.084	0.090	94.6
β_2^2	-1.749	-1.758	0.5	0.134	0.128	93.4	-1.763	0.8	0.140	0.137	94.9
γ_0^1	0.042	0.043	2.4	0.018	0.017	95.0	0.043	3.1	0.019	0.019	96.2
γ_1^1	-0.033	-0.033	0.1	0.016	0.017	96.3	-0.033	0.9	0.017	0.017	95.9
γ_2^1	-0.242	-0.244	0.9	0.026	0.026	95.2	-0.245	1.3	0.028	0.029	95.4
γ_0^2	-0.097	-0.099	1.6	0.038	0.037	95.5	-0.099	2.4	0.041	0.041	94.9
γ_1^2	-0.014	-0.014	0.7	0.018	0.019	95.5	-0.014	0.9	0.019	0.021	94.7
γ_2^2	-0.066	-0.065	2.0	0.040	0.039	93.7	-0.064	2.5	0.042	0.042	95.0
L(2,1)	0.333	0.334	0.3	0.054	0.054	95.2	0.335	0.7	0.057	0.058	94.7
L(3,1)	0.181	0.182	0.6	0.012	0.013	95.5	0.182	0.8	0.014	0.015	96.4
L(4,2)	0.066	0.066	0.8	0.013	0.013	95.5	0.067	1.2	0.015	0.014	94.8
L(3,3)	0.145	0.140	3.7	0.041	0.010	94.3	0.145	0.1	0.011	0.011	96.3
L(4,4)	0.247	0.246	0.4	0.027	0.015	94.5	0.247	0.0	0.016	0.016	94.7
α_{11}^0	-0.230	-0.231	0.6	0.016	0.016	95.1	-0.232	0.7	0.019	0.019	95.6
α_{11}^1	0.099	0.100	0.8	0.013	0.013	94.8	0.100	0.9	0.014	0.014	95.1
α_{12}^0	0.118	0.119	0.8	0.017	0.017	95.6	0.119	0.9	0.019	0.020	96.1
α_{12}^1	-0.040	-0.041	1.6	0.016	0.016	95.0	-0.041	2.4	0.018	0.019	96.2
α_{21}^0	0.095	0.096	1.4	0.020	0.020	95.1	0.097	1.7	0.022	0.022	94.3
α_{21}^1	0.043	0.042	1.6	0.022	0.023	95.2	0.042	1.9	0.025	0.024	93.9
α_{22}^0	-0.399	-0.400	0.3	0.027	0.026	93.6	-0.400	0.3	0.030	0.030	94.1
α_{22}^1	0.319	0.320	0.3	0.026	0.025	94.3	0.320	0.4	0.028	0.028	93.5
σ_1	0.397	0.399	0.5	0.014	0.014	95.2	0.399	0.6	0.015	0.015	95.3
σ_2	0.672	0.676	0.6	0.028	0.028	94.8	0.677	0.8	0.031	0.031	95.9
η_{01}	3.793	3.796	0.1	0.123	0.121	94.3	3.794	0.0	0.125	0.124	95.1
η_{11}	1.597	1.590	0.4	0.053	0.054	93.8	1.590	0.4	0.055	0.056	94.8
η_{02}	2.601	2.602	0.0	0.109	0.106	94.3	2.604	0.1	0.115	0.113	95.3
η_{12}	1.226	1.220	0.5	0.048	0.048	94.0	1.219	0.6	0.053	0.052	94.8

* (15% missing occasions, 7% missing outcomes)

[†] relative bias (%),

[‡] ASE is the asymptotic standard error, ESE is the empirical standard error and CR is the coverage rate of the 95% confidence interval.

Appendix C: Additional results in ADNI application

Table 5: Fixed effect estimates on baseline levels and changes of cerebral, cognitive and functional dimensions using a discretization step of 3 month.

Parameter	Cerebral dim.			Cognitive dim.			Functional dim.		
	θ	SE	p-value	θ	SE	p-value	θ	SE	p-value
<u>At baseline</u>									
Age (entry)	-0.534	0.067	< 0.001	-0.404	0.070	< 0.001	-0.013	0.073	0.857
Male	-0.183	0.081	0.025	-0.207	0.099	0.037	-	-	-
High. Educ.	-0.224	0.107	0.036	0.620	0.132	< 0.001	-	-	-
APOE	-0.252	0.086	0.003	-0.293	0.105	0.005	-0.122	0.098	0.216
MCI	-0.671	0.100	< 0.001	-1.693	0.137	< 0.001	-1.663	0.130	< 0.001
dAD	-1.412	0.127	< 0.001	-3.209	0.193	< 0.001	-3.770	0.194	< 0.001
<u>On the rate of change</u>									
Intercept	-0.091	0.028	0.001	0.143	0.102	0.162	-0.120	0.086	0.162
MCI	-0.068	0.035	0.049	-0.589	0.186	0.002	0.009	0.123	0.940
dAD	-0.237	0.095	0.012	-1.296	0.394	0.001	-0.558	0.280	0.047
Male	0.014	0.020	0.469	0.038	0.059	0.525	-	-	-
High. Educ.	-0.080	0.026	0.002	0.311	0.124	0.012	-	-	-
APOE	-0.100	0.021	<0.001	-0.194	0.067	0.004	-0.137	0.048	0.005

Table 6: Parameter estimates of the Cholesky decomposition of the variance-covariance matrix of overall random effects on baseline levels and changes of cerebral, cognitive and functional dimensions. Elements at 0 or 1 were fixed; standard errors of estimates are indicated in brackets below.

	u^A	u^C	u^F	v^A	v^C	v^F
u^A	1					
u^C	0.369 (0.051)	1				
u^F	0.167 (0.047)	0.256 (0.054)	1			
v^A	0.140 (0.032)	0	0	0.112 (0.012)		
v^C	0	0.562 (0.146)	0	0	0.001 (0.018)	
v^F	0	0	0.046 (0.060)	0	0	0.419 (0.041)

Table 7: Parameter estimates of the measurement model. Parameters ($\sigma_{Hip.}$, $\sigma_{zcortex.}$, $\sigma_{zmem.}$, $\sigma_{zlang.}$, $\sigma_{zexec.}$, $\sigma_{Faq.0}$) represent the standard deviation of the measurement errors for the 6 markers. Other parameters given by series of six ($\eta_{Hip.0}$ to $\eta_{Hip.5}$; $\eta_{zcortex.0}$ to $\eta_{zcortex.5}$; $\eta_{zmem.0}$ to $\eta_{zmem.5}$; $\eta_{zlang.0}$ to $\eta_{zlang.5}$; $\eta_{zexec.0}$ to $\eta_{zexec.5}$ and $\eta_{Faq.0}$ to $\eta_{Faq.4}$) correspond to the parameters of the quadratic I-splines link functions used to transform each marker (e.g., Hippocampal volume, Cortical thickness, Memory score, Language score, Executive functioning score, Functional autonomy score).

score	Parameter	Estimate	SE	p-value
Hippocampal volume	$\eta_{Hip.0}$	-8.556	0.489	<0.001
	$\eta_{Hip.1}$	0.716	0.220	0.001
	$\eta_{Hip.2}$	1.374	0.068	<0.001
	$\eta_{Hip.3}$	1.350	0.061	<0.001
	$\eta_{Hip.4}$	1.561	0.076	<0.001
	$\eta_{Hip.5}$	-0.709	0.664	0.286
	σ_{Hip}	1.906	0.082	< 0.001
Cortical thickness	$\eta_{zcortex.0}$	-5.239	0.231	<0.001
	$\eta_{zcortex.1}$	0.390	0.119	0.001
	$\eta_{zcortex.2}$	0.234	0.095	0.014
	$\eta_{zcortex.3}$	0.780	0.046	< 0.001
	$\eta_{zcortex.4}$	0.539	0.066	< 0.001
	$\eta_{zcortex.5}$	0.223	0.170	0.190
	$\sigma_{zcortex}$	0.253	0.009	< 0.001
Memory score	$\eta_{zmem.0}$	-7.962	0.374	< 0.001
	$\eta_{zmem.1}$	0.989	0.089	< 0.001
	$\eta_{zmem.2}$	1.093	0.065	< 0.001
	$\eta_{zmem.3}$	0.862	0.076	< 0.001
	$\eta_{zmem.4}$	0.927	0.086	< 0.001
	$\eta_{zmem.5}$	0.905	0.111	< 0.001
	σ_{zmem}	-1.516	0.067	< 0.001
Language score	$\eta_{zlang.0}$	-8.428	0.418	< 0.001
	$\eta_{zlang.1}$	0.154	0.192	0.421
	$\eta_{zlang.2}$	-8.182	1.146	0.463
	$\eta_{zlang.3}$	2.243	0.041	< 0.001
	$\eta_{zlang.4}$	1.827	0.064	< 0.001
	$\eta_{zlang.5}$	-1.998	0.995	0.045
	σ_{zlang}	1.151	0.056	< 0.001
Executive Functioning score	$\eta_{zexec.0}$	-8.351	0.428	< 0.001
	$\eta_{zexec.1}$	1.008	0.126	< 0.001
	$\eta_{zexec.2}$	0.568	0.130	< 0.001
	$\eta_{zexec.3}$	1.656	0.052	< 0.001
	$\eta_{zexec.4}$	1.125	0.100	< 0.001

Table 7 – *Continued from previous page*

score	Parameter	Estimate	SE	p-value
	$\eta_{zexec.5}$	0.467	0.333	0.160
	σ_{zexec}	1.401	0.067	< 0.001
	$\eta_{Faq.0}$	-7.726	0.314	< 0.001
	$\eta_{Faq.1}$	1.021	0.081	< 0.001
	$\eta_{Faq.2}$	0.269	0.140	0.054
Functional autonomy score	$\eta_{Faq.3}$	0.565	0.064	< 0.001
	$\eta_{Faq.4}$	0.687	0.041	< 0.001
	σ_{Faq}	0.657	0.027	< 0.001

Table 8: Estimates of the parameters of temporal influences on ADNI data when considering two discretization steps: 3 months (AIC = 29550.5) and 1.5 months (AIC = 29547.1). Superscripts 0, 1 and 2 refer to CN group, MCI group versus CN and dAD group versus CN, respectively.

	$\delta = 3$ months			$\delta = 1.5$ months		
	Estimate	SE	p-value	Estimate	SE	p-value
α_{AA}^0	-0.145	0.034	<0.001	-0.162	0.039	<0.001
α_{AA}^1	0.020	0.018	0.271	0.022	0.018	0.232
α_{AA}^2	0.002	0.025	0.946	0.002	0.027	0.932
α_{AC}^0	0.014	0.015	0.377	0.012	0.016	0.454
α_{AC}^1	0.048	0.018	0.008	0.050	0.019	0.008
α_{AC}^2	0.058	0.027	0.030	0.063	0.028	0.025
α_{AF}^0	0.015	0.031	0.627	0.016	0.031	0.606
α_{AF}^1	-0.023	0.032	0.478	-0.024	0.032	0.447
α_{AF}^2	-0.040	0.037	0.286	-0.047	0.038	0.212
α_{CA}^0	0.267	0.078	0.001	0.299	0.089	0.001
α_{CA}^1	0.016	0.060	0.792	0.014	0.062	0.817
α_{CA}^2	-0.049	0.080	0.535	-0.056	0.085	0.511
α_{CC}^0	-0.548	0.148	<0.001	-0.618	0.172	<0.001
α_{CC}^1	0.171	0.055	0.002	0.175	0.060	0.004
α_{CC}^2	0.115	0.076	0.132	0.117	0.083	0.159
α_{CF}^0	0.168	0.096	0.079	0.169	0.102	0.097
α_{CF}^1	-0.030	0.097	0.760	-0.020	0.103	0.846
α_{CF}^2	-0.034	0.113	0.766	-0.033	0.121	0.787
α_{FA}^0	0.114	0.045	0.012	0.114	0.045	0.011
α_{FA}^1	0.022	0.053	0.681	0.025	0.053	0.635
α_{FA}^2	-0.053	0.069	0.441	-0.052	0.070	0.455
α_{FC}^0	0.110	0.049	0.023	0.107	0.050	0.032
α_{FC}^1	0.021	0.053	0.696	0.030	0.054	0.584
α_{FC}^2	0.082	0.072	0.259	0.097	0.074	0.192
α_{FF}^0	-0.605	0.132	<0.001	-0.555	0.130	<0.001
α_{FF}^1	0.553	0.102	<0.001	0.492	0.097	<0.001
α_{FF}^2	0.402	0.106	<0.001	0.314	0.102	0.002

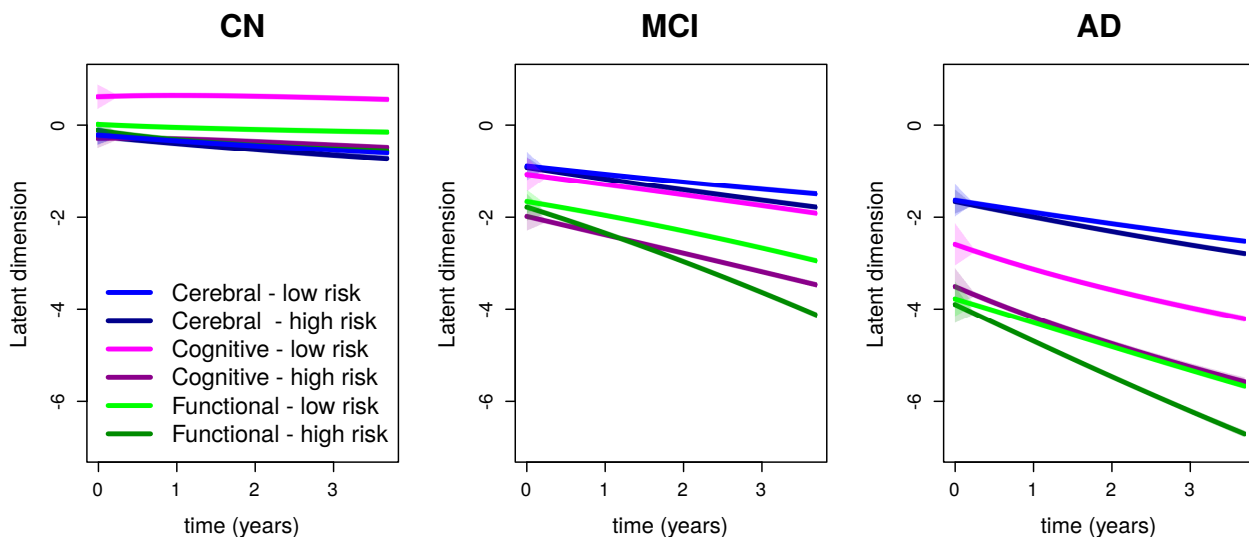


Figure 4: Predicted trajectories of cerebral anatomy, cognitive and functional dimensions at healthy (CN), mild cognitive impairment (MCI), and diagnosed with Alzheimer’s disease (AD) clinical stages of Alzheimer’s disease for a woman with a low risk of Alzheimer’s disease (non-carrier of APOE $\epsilon 4$ allele with higher educational level) and for a woman with a high risk of Alzheimer’s disease (carrier of APOE $\epsilon 4$ allele with lower educational level).

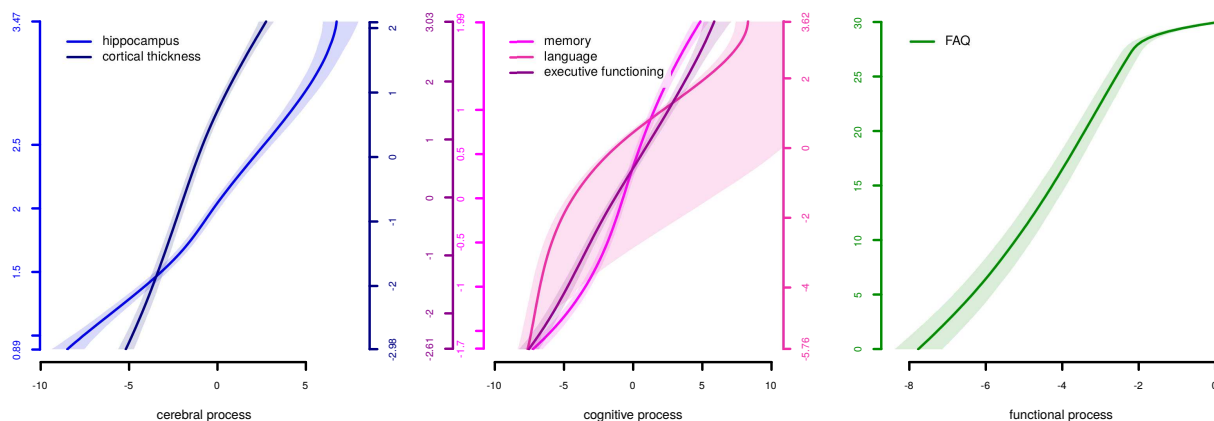


Figure 5: Estimated link functions (and 95% confidence bands obtained by 1000 Monte-Carlo draws) for markers Y_{hip} , Y_{cortic} , Y_{mem} , Y_{lang} , Y_{exec} and Y_{FAQ} (for mean hippocampal volume, mean regional cortical thickness, memory score, language score, executive functioning score and FAQ score).

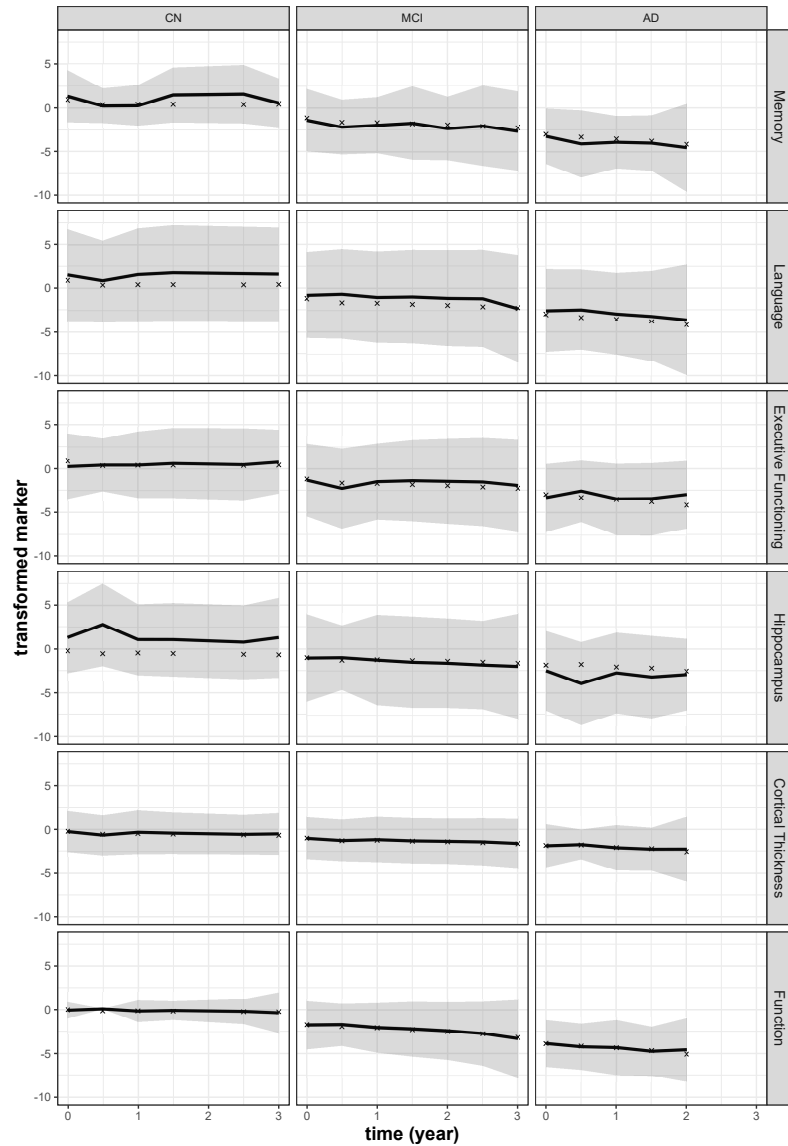


Figure 6: Mean transformed observed scores (plain lines) along with their 95% confidence interval (shadows) and corresponding mean subject-specific predictions (crosses) by protocol visit. Predictions are obtained using a 5-fold cross-validation technique. Columns refer to the group (controls CN, subjects with Mild Cognitive Impairments MCI and subjects diagnosed with Alzheimer’s disease dAD). Rows refer to the markers (e.g., memory score, language score, executive functioning score, mean hippocampal volume, mean regional cortical thickness and FAQ score) in their transformed scales (see Web Figure 3 for the plot of the estimated link functions between the natural scale and the transformed scale).

Table 2: Type-I error rates (in %) associated with each non diagonal element of the matrix of temporal influences \mathbf{A} when the matrix of temporal influences is generated approximately in continuous time ($\delta=0.001$) and estimated with discretization steps: $\delta=1/3$, $\delta=1/2$, $\delta=1$ for 2, 3 and 6 months respectively (1000 replicates; expected 95% interval [3.6, 6.4] for the nominal type-I error of 5%).

Parameter	$\delta = 1/3$	$\delta = 1/2$	$\delta = 1$
	\hat{r}		
a_{12}	5.4	4.9	6.5
a_{13}	5.3	5.3	8.6
a_{21}	5.6	6.0	7.5
a_{23}	4.7	6.0	4.1
a_{31}	5.4	5.2	7.1
a_{32}	4.5	4.8	4.8

Table 3: Estimates of the temporal influences between cerebral anatomy, cognitive ability and functional autonomy in ADNI1 using a discretization step of 3 months.

	Parameter		Estimate	SE	p-value
Influence on cerebral anatomy:					
Effect of cerebral anatomy	Intercept	α_{AA}^0	-0.145	0.034	< 0.001
	MCI	α_{AA}^1	0.020	0.018	0.271
	dAD	α_{AA}^2	0.002	0.025	0.946
Effect of cognitive ability	Intercept	α_{AC}^0	0.014	0.015	0.377
	MCI	α_{AC}^1	0.048	0.018	0.008
	dAD	α_{AC}^2	0.058	0.027	0.030
Effect of functional autonomy	Intercept	α_{AF}^0	0.015	0.031	0.627
	MCI	α_{AF}^1	-0.023	0.032	0.478
	dAD	α_{AF}^2	-0.040	0.037	0.286
Influence on cognitive ability:					
Effect of cerebral anatomy	Intercept	α_{CA}^0	0.267	0.078	< 0.001
	MCI	α_{CA}^1	0.016	0.060	0.792
	dAD	α_{CA}^2	-0.049	0.080	0.535
Effect of cognitive ability	Intercept	α_{CC}^0	-0.548	0.148	< 0.001
	MCI	α_{CC}^1	0.171	0.055	0.002
	dAD	α_{CC}^2	0.115	0.076	0.132
Effect of functional autonomy	Intercept	α_{CF}^0	0.168	0.096	0.079
	MCI	α_{CF}^1	-0.030	0.097	0.760
	dAD	α_{CF}^2	-0.034	0.113	0.766
Influence on functional autonomy:					
Effect of cerebral anatomy	Intercept	α_{FA}^0	0.114	0.045	0.012
	MCI	α_{FA}^1	0.022	0.053	0.681
	dAD	α_{FA}^2	-0.053	0.069	0.441
Effect of cognitive ability	Intercept	α_{FC}^0	0.111	0.049	0.023
	MCI	α_{FC}^1	0.021	0.053	0.696
	dAD	α_{FC}^2	0.082	0.072	0.259
Effect of functional autonomy	Intercept	α_{FF}^0	-0.605	0.133	< 0.001
	MCI	α_{FF}^1	0.553	0.102	< 0.001
	dAD	α_{FF}^2	0.403	0.106	< 0.001